

Robust Topology Optimization of Electric Machines using Topological Derivatives

Peter Gangl¹ Theodor Komann² Nepomuk Krenn¹
 Stefan Ulbrich²

¹RICAM, Austrian Academy of Sciences,
 Altenberger Straße 69, 4040 Linz, Austria

²Department of Mathematics, TU Darmstadt,
 Dolivostraße 15, 64297 Darmstadt, Germany

Abstract

Designing high-performance electric machines that maintain their efficiency and reliability under uncertain material and operating conditions is crucial for industrial applications. In this paper, we present a novel framework for robust topology optimization with partial differential equation constraints to address this challenge. The robust optimization problem is formulated as a min-max optimization problem, where the inner maximization is the worst case with respect to predefined uncertainties, while the outer minimization aims to find an optimal topology that remains robust under these uncertainties using the topological derivative. The shape of the domain is represented by a level set function, which allows for arbitrary perturbation of the domain. The robust optimization problem is solved using a theorem of Clarke to compute subgradients of the worst case function. This allows the min-max problem to be solved efficiently and ensures that we find a design that performs well even in the presence of uncertainty. Finally, numerical results for a two-material permanent magnet synchronous machine demonstrate both the effectiveness of the method and the improved performance of robust designs under uncertain conditions.

1 Introduction

Electric machines play an important role in modern industrial applications, including automotive, aerospace, and renewable energy systems [20]. In light of recent regulatory developments—such as the European Union’s approval of a 2035 phaseout of CO₂-emitting vehicles—these machines are expected to become even

more important in achieving the transition towards sustainable mobility. Consequently, various factors such as efficiency, performance and manufacturability must be carefully considered when designing these machines. In this context, topology optimization with the consideration of constraints is a popular and useful technique for designing electric machines with the goal of finding optimal material distribution, leading to improved performance and reduced material costs [39, 21, 33, 43]. Topology optimization methodologies can be broadly split into two types: genetic and gradient-based. Genetic optimization algorithms have been extensively applied to topology optimization of electric machines due to their ability to explore complex design spaces without requiring derivative information [44, 10]. An advantage of genetic algorithms is the ability to bypass local minima, thereby increasing the likelihood of finding global minima. This is especially useful for topology optimization, where many locally minimal designs are common. However, these methods are black-box algorithms, have a small and by parametrization restricted design space and can require prohibitively long computation times, which can take days or even weeks. Since our application involves an electric machine with an advanced design space because the physical system is described by a PDE, we will use a derivative-based algorithm in this work. Such an approach can use sensitivity information, allowing us to efficiently explore the design space and avoid the extensive computational costs associated with genetic methods.

Derivative-based topology optimization methods can be classified into density-based and level set approaches. Density-based methods represent the design by a density variable taking values between 0 and 1 and interpolate material properties accordingly. The density-based topology optimization in the field of electromagnetism was introduced by Dyck and Lowther in 1996 [18], building on earlier foundational work by Bendsoe in 1989, who described topology optimization as a problem of distributing materials first [7]. One prominent approach is the *Solid Isotropic Material with Penalization* (SIMP) method, where intermediate material densities are penalized due to their nonphysical behavior. Recently in [12] this was successfully applied in multi-material topology optimization using Wachspress interpolation techniques for the design of a 3-phase electrical machine, addressing challenges such as numerical instabilities and sensitivity filtering. Moreover, the density method has been effectively used to optimize electric machines in [28, 33]. It is well established and can lead to efficient electromagnetic designs, but choosing an appropriate interpolation function can be challenging, especially when dealing with nonlinear or multi physical problems [43]. In contrast level set methods represent the material distribution and topology using a level set function that implicitly defines different material phases and thus divides the design domain into separate subdomains. In topology optimization, the evolution of this level set function can be achieved by computing sensitivities, such as shape derivatives or shape gradients, which are inserted into the Hamilton-Jacobi equation [2] or by the topological derivative [22, 3]. We will use the level set ap-

proach with the topological derivative in this work, as it offers great flexibility for changing the initial design and is well-suited for electric machines due to its ability to precisely define material interfaces and explore complex geometries.

While all these approaches have improved electric machine design, a major gap remains: they often fail to address robustness with respect to manufacturing tolerances and parameter uncertainties. Such uncertainties are important in practice, since even small geometric deviations or variations in material properties can worsen the performance and cause a design that appears optimal in theory to perform poorly in reality [36, 5]. There are two main approaches to handle these uncertainties. The first is to consider a stochastic optimization problem, which assumes that uncertainty can be described probabilistically. This approach minimizes the expected value of an objective function, as discussed in [46, 9] and for optimization problems constrained by a partial differential equation (PDE), in [31, 25]. The second, more conservative approach is robust optimization, introduced by Ben-Tal and Nemirovski [5], which minimizes the worst case objective over a predefined uncertainty set. This deterministic approach has the advantage of ensuring good performance even under the most unfavorable realization of uncertainties. In some engineering applications, ensuring such worst case performance is more desirable than only being robust in terms of the expected value. The uncertainty affecting our model comes from two main sources: Imperfections in achieving the desired design variables, commonly referred to as *implementation errors* $\delta x \in U_x$, and *parameter uncertainties* $q \in U_q$, which result from inaccuracies in the problem formulation, such as noise [8]. These sets are combined into a Cartesian product to form the overall uncertainty set: $U = U_q \times U_x$, which is closed, convex, and bounded. If x is our design variable, the robust optimization problem can be formulated as:

$$\min_x \max_{(\delta x, q) \in U} g(x + \delta x, q), \quad (1)$$

Here, $g(x + \delta x, q)$ typically measures the performance of the quantity of interest (e.g., average torque or torque ripple in electric machines) for a given design x perturbed by implementation errors δx and parameter uncertainties q . Therefore the worst case function can be written as

$$f(x) = \max_{(\delta x, q) \in U} g(x + \delta x, q) \quad (2)$$

Methods to solve this problem will be presented in Section 3.3. Figure 1 illustrates the worst case function and the difference between a robust and a global minimum, with the left subfigure showing uncertainty in the parameter q , and the right subfigure showing on uncertainty in the design δx . This robust perspective is crucial for electric machines, as ignoring uncertainties in parameter or shape can yield designs that are highly sensitive to small perturbations[1, 29, 34, 30, 15]. These uncertainties arise from variations in physical parameters and geometric

shapes. To address uncertainties in material properties, [41] applied generalized polynomial chaos expansions. This method results in electric machine designs that maintain high performance even when material properties change. Similar observations have been made in other engineering applications. Consequently, robust optimization techniques have been applied to other topology optimization problems. In density based topology optimization, such as for airwing structures, incorporating uncertainties into the optimization problem has resulted in designs that are not only more robust but also more practical for real-world use [47]. Another example for topology optimization under uncertainty can be found in [14], who proposed a method for risk-averse shape optimization of elastic structures with uncertain loads. Their approach uses different scenarios to calculate the likelihood of design failure and applies a smooth gradient method to change the shape, allowing new structures to form. [38] used stochastic collocation together with a level set method for robust shape optimization in linear elasticity to handle uncertainties in loading and material properties. Similarly, [49] introduced a non-probabilistic robust topology optimization technique using interval uncertainty, where they estimate the worst case with interval arithmetic. In this paper, we present a novel robust topology optimization algorithm that combines a robust optimization technique developed in [30], which is based on [8], with a level set algorithm that applies the topological derivative [32]. This combination allows us to efficiently solve robust topology optimization problems formulated as min-max problems, where inner maximization calculates the worst case with respect to predefined uncertainties, while the outer minimization uses the topological derivative to minimize the worst case. We illustrate our technique in a concrete engineering problem by applying it to the robust design optimization of an electric machine.

The remainder of this paper is organized as follows. Section 2 presents the physical model of the robust topology optimization problem. Section 3 describes the main algorithmic steps and mathematical theory of both topology optimization and robust optimization. Section 4 combines these ideas into a unified approach to robust topology optimization using the topological derivative. Section 5 provides numerical results for a two-material PMSM, highlighting the advantages of our method. Finally, Section 6 concludes the paper and discusses potential directions for future research.

1.1 Notation

In this paper we will use standard notation for function spaces $C(D)$, $C_c^\infty(D)$, $L_2(D)$, $H^1(D)$ where $D \subset \mathbb{R}^2$ is an open domain. These space refer to continuous, smooth and compactly supported, square integrable and functions with square integrable weak first derivatives, respectively. Further we denote by $\text{curl} v = (\partial_y v, -\partial_x v)^T$ the scalar-to-vector curl differential operator, $\widehat{\text{curl}} = -\partial_y v_x + \partial_x v_y$ is the vector-to-scalar curl and $e_\varphi = (\cos \varphi, \sin \varphi)^T \in \mathbb{R}^2$ the unit vector with

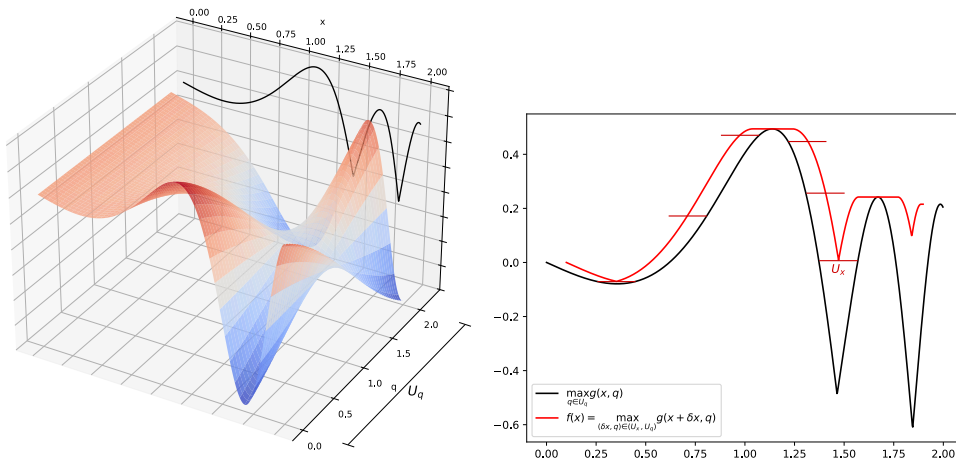


Figure 1: Example of a function $g(x, q)$ with worst case $\max_{q \in U_q}$ in black (left); worst case w.r.t. q (black) and w.r.t. $(\delta x, q)$, i.e. $f(x) = \max_{(\delta x, q) \in (U_x, U_q)} g(x + \delta x, q)$ (right).

angle φ from the positive x -axis. We use the open Euclidean unit ball $B_\epsilon(z) := \{x \in \mathbb{R}^2 : \|x - z\|_2 < \epsilon\}$ and denote by χ_Ω the characteristic function of Ω . By $v|_D$ we denote the restriction of the function v to the domain D . The function $\rho_\alpha : \mathbb{R} \rightarrow \mathbb{R}, \rho_\alpha(x, y) = R_\alpha(x, y)^T$ is the rotational coordinate transformation with the rotation matrix $R_\alpha = (e_\alpha, e_{\alpha + \frac{\pi}{2}})$.

2 Physical Model

We consider a permanent magnet synchronous machine in static operation, see Figure 2 (left). The alternating source current which is impressed in the stator coils D_A, D_B, D_C , depicted in yellow, creates a rotating magnetic field. The interaction of this field with the field caused by the permanent magnets $D_{\text{magnet}1}$ (light blue), $D_{\text{magnet}2}$ (light green) produces a torque transferred by the shaft of the machine. Further we consider in our material model saturation effects leading to a nonlinear equation. Since the iron parts $D_{\text{stator}}, \Omega_f$ (red) consist of thin isolated sheets stacked in axial direction, considering only a 2d cross section is a common approximation in electric machine optimization. Due to the periodicity of the design, the alternating directions of the permanent magnets and the antiperiodicity of the excitation currents the resulting fields are antiperiodic by one pole. It is therefore sufficient to consider a 45° piece of the machine, see Figure 2 (right) as the computational domain imposing antisymmetric boundary conditions. These simplifications lead to the commonly used nonlinear magnetostatic approximation of the Maxwell's equations, i.e., to find the third component of

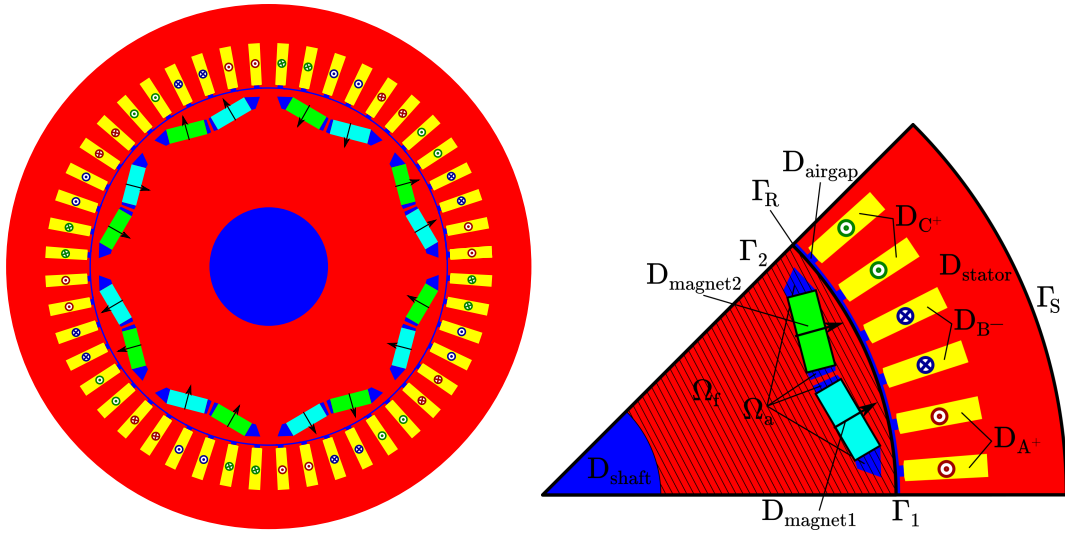


Figure 2: Left: 2d cross section of permanent magnet synchronous machine: Rotor and stator iron in red, coils in yellow with phase distribution (A: red, B: blue, C: green), permanent magnets with magnetization direction in light blue and light green, airgap, airpockets and shaft in blue. Right: One pole of the machine, the computational domain D_{all} . Design domain D (dashed area) consisting of rotor iron $\Omega_f \subseteq D$ (red) and rotor air $\Omega_a \subseteq D$ (blue). Rotor D_R consisting of shaft D_{shaft} , design domain D and permanent magnets $D_{\text{magnet1}}, D_{\text{magnet2}}$ with outer boundary Γ_R . Stator D_S consisting of airgap D_{airgap} , iron D_{stator} and coils $D_{A^+}, D_{B^-}, D_{C^+}$ with outer boundary Γ_S . Boundaries of pole Γ_1, Γ_2 .

the magnetic vector potential $u \in H^1(D_{\text{all}})$ with

$$\begin{aligned} \widetilde{\text{curl}} h_{\Omega}(\text{curl} u, q) &= j(q) && \text{in } D_{\text{all}} \\ u &= 0 && \text{on } \Gamma_S \\ u|_{\Gamma_1} &= -u|_{\Gamma_2} \end{aligned} \quad (3)$$

where $j(q) = j_A(q)\chi_{D_{A^+}} - j_B(q)\chi_{D_{B^-}} + j_C(q)\chi_{D_{C^+}} \in L_2(D_{\text{all}})$ is the three phase source current and q is a parameter which may be uncertain. By $\Omega := (\Omega_f, \Omega_a)$ we denote the distribution of iron and air in the design domain D . The magnetic material law h_{Ω} defining the relation between magnetic flux $b = \text{curl} u$ and magnetic field $h = h_{\Omega}(b, q)$ is given piecewise

$$\begin{aligned} h_{\Omega}(b, q) &= h(\Omega, b, q)\chi_D + h_f(b, q)\chi_{D_{\text{stator}}} + h_a(b, q)\chi_{D_{A^+} \cup D_{B^-} \cup D_{C^+} \cup D_{\text{shaft}} \cup D_{\text{airgap}}} \\ &\quad + h_{m_1}(b, q)\chi_{D_{\text{magnet1}}} + h_{m_2}(b, q)\chi_{D_{\text{magnet2}}} \end{aligned} \quad (4)$$

with $h(\Omega, b, q) = h_f(b, q)\chi_{\Omega_f} + h_a(b, q)\chi_{\Omega_a}$. The choice of the material laws h_f, h_a, h_m and the influence of the uncertain parameter q will be specified in the section of numerical results, Section 5. In order to be able to solve the magnetostatic equation (3) for a rotor rotated by an arbitrary angle α we use the harmonic mortar approach from [19]. We allow u_{α} to be discontinuous at the interface Γ_R and introduce a Lagrange multiplier λ_{α} to reinforce continuity in the potentially rotated setting: Find $(u_{\alpha}, \lambda_{\alpha}) \in \mathcal{H} \times \mathcal{L}$ with

$$\begin{aligned} \int_{D_{\text{all}}} h_{\Omega}(\text{curl} u_{\alpha}, q) \cdot \text{curl} v \, dx + \langle \lambda_{\alpha}, (v|_{D_S} - v|_{D_R} \circ \rho_{-\alpha}) \rangle_{\Gamma_R} &= \int_{D_{\text{all}}} j(\alpha, q) v \, dx \\ \langle \mu, (u_{\alpha}|_{D_S} - u|_{D_R} \circ \rho_{-\alpha}) \rangle_{\Gamma_R} &= 0 \end{aligned} \quad (5)$$

for all $(v, \mu) \in \mathcal{H} \times \mathcal{L}$ with $\mathcal{H} = \{v : v|_{D_R} \in H^1(D_R), v|_{D_S} \in H^1(D_S), v|_{\Gamma_S} = 0, v|_{\Gamma_1} = -v|_{\Gamma_2}\}$, $\mathcal{L} = H^{-\frac{1}{2}}(\Gamma_R)$. Based on energy considerations the torque produced by magneto-mechanical energy conversion can be computed by

$$\mathcal{T}(\alpha) = T(u_{\alpha}, \lambda_{\alpha}, \alpha) = r_{\Gamma_R} \langle \lambda_{\alpha}, (\text{curl} u_{\alpha} \cdot n_{\Gamma_R}) \circ \rho_{-\alpha} \rangle_{\Gamma_R} \quad (6)$$

with r_{Γ_R} the radius and n_{Γ_R} the outer unit normal vector of the rotor. In the sequel we are interested in the average torque. Since the state $(u_{\alpha}, \lambda_{\alpha})$ is periodic by mechanical rotations of 15° we consider N equidistant rotor positions

$$\alpha^n = \frac{15^\circ n}{N}, n = 0, \dots, N-1 \quad (7)$$

within this period. We denote by $(u^n, \lambda^n) := (u_{\alpha^n}, \lambda_{\alpha^n})$ the solution of (5) for the rotor position α^n .

Remark 1. The differential operators $\widetilde{\text{curl}}$, curl introduced in Section 1.1 correspond to rotated versions of div , ∇ , respectively. For an isotropic material law, i.e. $h_\Omega(b_1, q) = h_\Omega(b_2, q)$ for all $b_1, b_2 \in \mathbb{R}^2$ with $|b_1| = |b_2|$, problem (3) corresponds to a nonlinear diffusion equation

$$\widetilde{\text{curl}}h_\Omega(\text{curl}u, q) = -\text{div}h_\Omega(\nabla u, q),$$

with suitable boundary conditions.

Remark 2. The formula for the torque (6) is derived in [19]. There are strong similarities to the widely used torque calculation method based on the Maxwell stress tensor [42],

$$T = \int_S \frac{1}{\mu_0} B_r B_t r \, dS,$$

where μ_0 is the magnetic vacuum permeability, B_r and B_t are the radial and normal component of the magnetic flux density B and S is a circle in the airgap. In our formula the Lagrange multiplier λ represents the tangential component of the magnetic field $h \cdot t_{\Gamma_R} \sim \mu_0^{-1} B_t$ and $\text{curl}u \cdot n_{\Gamma_R} = b \cdot n_{\Gamma_R} \sim B_r$. Similarly the domain of integration $\Gamma_R \subset D_{\text{airgap}}$ is a circle in the airgap.

Remark 3. In [19] the authors propose to use harmonic basis functions to discretize the space of Lagrange multipliers \mathcal{L} which is also done in this work. However, to guarantee unique solvability one needs to fulfill a discrete inf-sup condition which results in a limitation of the degrees of freedom of the discrete space.

3 Methodology

Although our theoretical considerations hold generally, we choose a model problem to develop our methodology.

3.1 Model Optimization Problem

Based on the forward problem introduced in Section 2 we aim to find a design Ω which maximizes the average torque of the machine for some parameter q . This leads to the following PDE constrained optimization problem:

$$\begin{aligned} \min_{\Omega} & -\frac{1}{N} \sum_{n=0}^{N-1} T(u^n, \lambda^n, \alpha^n) \\ \text{s.t.} & e(\Omega, q, \alpha^n, (u^n, \lambda^n)) = 0, \quad n = 0, \dots, N-1, \end{aligned} \tag{8}$$

where T is the torque (6) and e is the nonlinear magnetostatic PDE (5) for material configuration Ω , parameter q and rotor position α^n . For a given design

Ω and parameter q we denote by $(u^n(\Omega, q), \lambda^n(\Omega, q)) \in \mathcal{H} \times \mathcal{L}$ the unique solution of $e(\Omega, q, \alpha^n, (u, \lambda)) = 0$. The reduced cost functional of the parametrized design optimization problem is defined as

$$\mathcal{J}(\Omega, q) := -\frac{1}{N} \sum_{n=0}^{N-1} T(u^n(\Omega, q), \lambda^n(\Omega, q), \alpha^n). \quad (9)$$

The Lagrangian of problem (8) is given by

$$\begin{aligned} \mathcal{G}(\Omega, q, (\alpha^0, \dots, \alpha^{N-1}), (u^0, \dots, u^{N-1}, \lambda^0, \dots, \lambda^{N-1}), (p^0, \dots, p^{N-1}, \eta^0, \dots, \eta^{N-1})) = \\ -\frac{1}{N} \sum_{n=0}^{N-1} T(u^n, \lambda^n, \alpha^n) + \sum_{n=0}^{N-1} \langle e(\Omega, q, \alpha^n, (u^n, \lambda^n)), (p^n, \eta^n) \rangle. \end{aligned} \quad (10)$$

Since we will apply gradient based methodologies to solve the optimization problem (8), we introduce the adjoint states $(p^n, \eta^n) \in \mathcal{H} \times \mathcal{L}$, which solve the adjoint equation, obtained by differentiation of the Lagrangian (10) with respect to the state (u^n, λ^n) ,

$$\begin{aligned} \int_{D_{\text{all}}} \partial_b h_{\Omega}(\text{curl} u^n, q) \text{curl} p^n \cdot \text{curl} v^n \, dx + \langle \eta^n, (v^n|_{D_S} - v^n|_{D_R} \circ \rho_{-\alpha^n}) \rangle_{\Gamma_R} \\ = \frac{r_{\Gamma_R}}{N} \langle \lambda^n, (\text{curl} v^n \cdot n_{\Gamma_R}) \circ \rho_{-\alpha^n} \rangle_{\Gamma_R} \quad (11) \\ \langle \mu^n, (p^n|_{D_S} - p^n|_{D_R} \circ \rho_{-\alpha^n}) \rangle_{\Gamma_R} = \frac{r_{\Gamma_R}}{N} \langle \mu, (\text{curl} u^n \cdot n_{\Gamma_R}) \circ \rho_{-\alpha^n} \rangle_{\Gamma_R} \end{aligned}$$

for all $(v^n, \mu^n) \in \mathcal{H} \times \mathcal{L}, n = 0, \dots, N-1$.

3.2 Topology Optimization

In this subsection we consider a fixed parameter q and, for the sake of readability, skip it by writing $\mathcal{J}(\Omega)$ instead of $\mathcal{J}(\Omega, q)$. We denote the configuration of iron and air in the rotor by $\Omega = (\Omega_f, \Omega_a) \in \mathcal{E}$, where Ω_f, Ω_a are open and disjoint subsets of the design domain D with $\overline{\Omega_f} \cup \overline{\Omega_a} = \overline{D}$. Here, $\mathcal{E} = E \times E$ denotes the set of admissible configurations where E is the set of Lipschitz subsets of D with a uniform Lipschitz constant L_E , which allows to prove existence of a minimizer, see also [27, 23]. We will use the notation $z \in \Omega \Leftrightarrow z \in \Omega_f \cup \Omega_a$ to indicate that a point z is in D but not at the interface between Ω_f and Ω_a . The sensitivity of \mathcal{J} to circular topological perturbations $\omega_{\epsilon}(z) := \epsilon\omega + z$, see Figure 3, is given by the topological derivative. For perturbations of iron by including air the topological derivative is defined by

$$\frac{d^{f \rightarrow a}}{d\Omega} \mathcal{J}(\Omega)(z) := \lim_{\epsilon \searrow 0} \frac{\mathcal{J}(\Omega_{\epsilon}(z)) - \mathcal{J}(\Omega)}{|\omega_{\epsilon}(z)|}, \Omega_{\epsilon}(z) = (\Omega_f \setminus \overline{\omega_{\epsilon}(z)}, \Omega_a \cup \overline{\omega_{\epsilon}(z)}) \quad (12)$$

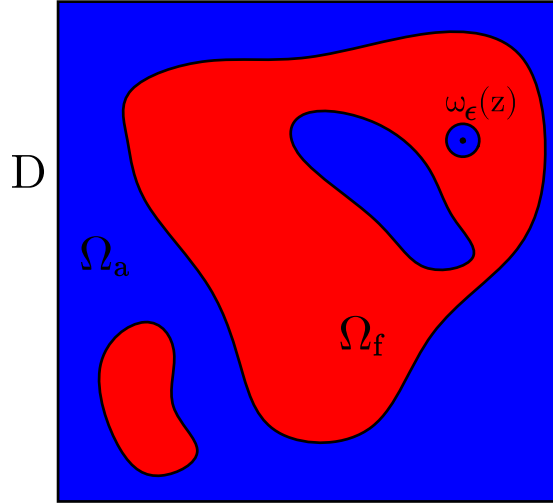


Figure 3: Some design domain D consisting of two materials air in Ω_a and iron in Ω_f . Perturbation of Ω_f by putting air in $\omega_\epsilon(z)$.

for $z \in \Omega_f$, and for changes from air to iron in points $z \in \Omega_a$ by interchanging the role of iron (index f) and air (index a). Combining these two, we get the topological derivative for $z \in \Omega$,

$$\frac{d}{d\Omega} \mathcal{J}(\Omega)(z) = \begin{cases} \frac{d^{f \rightarrow a}}{d\Omega} \mathcal{J}(\Omega)(z) & \text{if } z \in \Omega_f, \\ \frac{d^{a \rightarrow f}}{d\Omega} \mathcal{J}(\Omega)(z) & \text{if } z \in \Omega_a. \end{cases} \quad (13)$$

Based on this we will use the following term of optimality [3]:

Definition 1. A configuration $\Omega \in \mathcal{E}$ is called locally optimal with respect to topological perturbations if

$$\frac{d}{d\Omega} \mathcal{J}(\Omega)(z) \geq 0 \text{ for } z \in \Omega. \quad (14)$$

3.2.1 Evaluation of the Topological Derivative

The topological derivative for problems constrained by the magnetostatic PDE was first derived in [4]. To evaluate its formula in a systematic way we apply the framework of [24]. For a point $z \in \Omega$ we use the abbreviation $U_z^n = \text{curl} u^n(z)$ and $P_z^n = \text{curl} p^n(z)$ for point evaluation of the state u^n coming from (5) and the adjoint state p^n coming from (11), respectively. First we introduce the first order asymptotic corrector of the state subject to topological perturbations $K_U \in BL(\mathbb{R}^2) := \{v \in L_2^{loc}(\mathbb{R}^2) : \nabla v \in L_2(\mathbb{R}^2)^2\} / \mathbb{R}$ which is the solution of the the

auxiliary exterior problem for $U \in \mathbb{R}^2$

$$\begin{aligned} \int_{\mathbb{R}^2} (h_\omega^{f \rightarrow a}(\xi, \text{curl}K_U(\xi) + U) - h_\omega^{f \rightarrow a}(\xi, U)) \cdot \text{curl}v(\xi) \, d\xi \\ = - \int_\omega (h_a(U) - h_f(U)) \cdot \text{curl}v(\xi) \, d\xi \end{aligned} \quad (15)$$

for all $v \in BL(\mathbb{R}^2)$ with $\omega = B_1(0)$ and $h_\omega^{f \rightarrow a}(\xi, b) = h_a(b)\chi_\omega(\xi) + h_f(b)\chi_{\mathbb{R}^2 \setminus \bar{\omega}}(\xi)$. The topological derivative for material changes from iron to air, i.e. $z \in \Omega_f$, is then given by

$$\begin{aligned} \frac{d^{f \rightarrow a}}{d\Omega} \mathcal{J}(\Omega)(z) = \\ \sum_{n=0}^{N-1} \left(\frac{1}{|\omega|} \int_{\mathbb{R}^2} (h_\omega^{f \rightarrow a}(\xi, \text{curl}K_{U_z^n}(\xi) + U_z^n) - h_\omega^{f \rightarrow a}(\xi, U_z^n) - \partial_b h_\omega^{f \rightarrow a}(\xi, U_z^n) \text{curl}K_{U_z^n}(\xi)) \cdot P_z^n \, d\xi \right. \\ \left. + \frac{1}{|\omega|} \int_\omega (\partial_b h_a(U_z^n) - \partial_b h_f(U_z^n)) \text{curl}K_{U_z^n}(\xi) \cdot P_z^n \, d\xi \right. \\ \left. + (h_a(U_z^n) - h_f(U_z^n)) \cdot P_z^n \right), \end{aligned} \quad (16)$$

where only the piecewise defined material law $h_\omega^{f \rightarrow a}$ and $K_{U_z^n}$ depend on ξ and $U_z^n, P_z^n \in \mathbb{R}^2$ are constant. If the material laws are both linear of the form

$$h_f(b) = \nu_f b, h_a(b) = \nu_0 b, \quad (17)$$

the exterior problem (15) has an analytical solution

$$-\frac{\nu_0 - \nu_f}{\nu_0 + \nu_f} U \cdot \left(\xi \chi_\omega(\xi) + \frac{\xi}{|\xi|^2} \chi_{\mathbb{R}^2 \setminus \bar{\omega}}(\xi) \right) \quad (18)$$

which leads to the topological derivative formula

$$\frac{d^{f \rightarrow a}}{d\Omega} \mathcal{J}(\Omega)(z) = \sum_{n=0}^{N-1} 2\nu_0 \frac{\nu_0 - \nu_f}{\nu_0 + \nu_f} U_z^n \cdot P_z^n. \quad (19)$$

Remark 4. For linear material laws the evaluation of the topological derivative is straightforward. In the nonlinear case one theoretically has to solve the exterior problem (15) for every point $z \in \Omega$, rotor position n depending on the current design Ω . However, since the topological derivative depends only on $U_z^n = \text{curl}u^n(z) \in \mathbb{R}^2$ and $P_z^n = \text{curl}p^n(z) \in \mathbb{R}^2, z \in \Omega, n = 0, \dots, N - 1$ it is convenient to take samples for all possible $U \in \mathbb{R}^2, P \in \mathbb{R}^2$ and to interpolate them. First we note, that formula (20) depends on P_z^n in a linear way, therefore it is sufficient to consider only the base vectors of \mathbb{R}^2 , e_0, e_{τ_2} , for P . Further it was

shown in [4] that due to the isotropic characteristic of the material laws h_f, h_a the topological derivative can be written as

$$\frac{d^{f \rightarrow a}}{d\Omega} \mathcal{J}(\Omega)(z) = \sum_{n=0}^{N-1} \begin{pmatrix} \cos \beta_z^n & -\sin \beta_z^n \\ \sin \beta_z^n & \cos \beta_z^n \end{pmatrix} \begin{pmatrix} f_1^{f \rightarrow a}(|U_z^n|) \\ f_2^{f \rightarrow a}(|U_z^n|) \end{pmatrix} \cdot P_z^n, \beta_z^n = \arccos \frac{U_z^n \cdot e_0}{|U_z^n|} \quad (20)$$

with

$$\begin{aligned} f_1^{f \rightarrow a}(t) &= \frac{1}{|\omega|} \int_{\mathbb{R}^2} (h_\omega^{f \rightarrow a}(\xi, \text{curl}K_{te_0}(\xi) + te_0) - h_\omega^{f \rightarrow a}(\xi, te_0) - \partial_b h_\omega^{f \rightarrow a}(\xi, te_0) \text{curl}K_{te_0}(\xi)) \cdot e_0 d\xi \\ &\quad + \frac{1}{|\omega|} \int_{\omega} (\partial_b h_a(te_0) - \partial_b h_f(te_0)) \text{curl}K_{te_0}(\xi) \cdot e_0 d\xi \\ &\quad + (h_a(te_0) - h_f(te_0)) \cdot e_0, \\ f_2^{f \rightarrow a}(t) &= \frac{1}{|\omega|} \int_{\mathbb{R}^2} (h_\omega^{f \rightarrow a}(\xi, \text{curl}K_{te_0} + te_0) - h_\omega^{f \rightarrow a}(\xi, te_0) - \partial_b h_\omega^{f \rightarrow a}(\xi, te_0) \text{curl}K_{te_0}(\xi)) \cdot e_{\frac{\pi}{2}} d\xi \\ &\quad + \frac{1}{|\omega|} \int_{\omega} (\partial_b h_a(te_0) - \partial_b h_f(te_0)) \text{curl}K_{te_0}(\xi) \cdot e_{\frac{\pi}{2}} d\xi \\ &\quad + (h_a(te_0) - h_f(te_0)) \cdot e_{\frac{\pi}{2}}. \end{aligned} \quad (21)$$

It is therefore convenient to take samples $f_{1,k}^{f \rightarrow a} = f_1^{f \rightarrow a}(t_k)$, $f_{2,k}^{f \rightarrow a} = f_2^{f \rightarrow a}(t_k)$ for $0 = t_1 < t_2 < \dots < t_K = t_{\max}$ of formula (21) (which includes solving the exterior problem (15) for $U = t_k e_0$) in an offline phase and providing an interpolation

$$\tilde{f}_1^{f \rightarrow a}, \tilde{f}_2^{f \rightarrow a}. \quad (22)$$

which gets evaluated online when computing the topological derivative using (20).

Remark 5. The topological derivative from air to iron $\frac{d^{a \rightarrow f}}{d\Omega}$ can be computed by applying the same formula (16) but interchanging the role of the materials, i.e. interchanging h_f and h_a . Note that this also requires the solution of the modified version of (15).

Remark 6. Note that, although we skipped the uncertainty q in this subsection, all material laws may depend on the parameter by $h(b) = h(b, q)$, therefore also the topological derivative depends on q including the precomputed functions $f_1^{f \rightarrow a}(t, q)$, $f_2^{f \rightarrow a}(t, q)$, $f_1^{a \rightarrow f}(t, q)$, $f_2^{a \rightarrow f}(t, q)$.

3.2.2 Level Set Algorithm

This methodology on how to update the design defined by a level set function using the topological derivative was introduced in [3]. We represent the configu-

ration Ω by a continuous level set function $\psi \in \mathcal{S}$

$$\begin{aligned}\psi(z) &> 0 \Leftrightarrow z \in \Omega_f \\ \psi(z) &= 0 \Leftrightarrow z \in \overline{\Omega_f} \cap \overline{\Omega_a} \\ \psi(z) &< 0 \Leftrightarrow z \in \Omega_a\end{aligned}\tag{23}$$

with $\mathcal{S} \subset \{\psi \in C(D) : \|\psi\|_{L_2(D)} = 1\}$ the space of admissible level set functions. Next we introduce the generalized topological derivative

$$g_\Omega(z) = \begin{cases} \frac{d^{f \rightarrow a}}{d\Omega} \mathcal{J}(\Omega)(z) & \text{if } z \in \Omega_f \\ -\frac{d^{a \rightarrow f}}{d\Omega} \mathcal{J}(\Omega)(z) & \text{if } z \in \Omega_a. \end{cases}\tag{24}$$

This is motivated by the following lemma

Lemma 1. *The configuration $(\Omega_f, \Omega_a) = \Omega_\psi$, described by a level set function $\psi \in \mathcal{S}$ is (locally) optimal with respect to topological perturbations if*

$$\psi(z) = \frac{g_{\Omega_\psi}(z)}{\|g_{\Omega_\psi}\|_{L_2(D)}}\tag{25}$$

for all $z \in \Omega_\psi$.

Proof. Let $z \in \Omega_f$. Then we conclude

$$z \in \Omega_f \Leftrightarrow 0 < \psi(z) = \frac{g_{\Omega_\psi}(z)}{\|g_{\Omega_\psi}\|_{L_2(D)}} \Leftrightarrow g_{\Omega_\psi}(z) > 0 \Leftrightarrow \frac{d^{f \rightarrow a}}{d\Omega} \mathcal{J}(\Omega)(z) > 0.$$

Similarly we get for $z \in \Omega_a$

$$z \in \Omega_a \Leftrightarrow 0 > \psi(z) = \frac{g_{\Omega_\psi}(z)}{\|g_{\Omega_\psi}\|_{L_2(D)}} \Leftrightarrow g_{\Omega_\psi}(z) < 0 \Leftrightarrow \frac{d^{a \rightarrow f}}{d\Omega} \mathcal{J}(\Omega)(z) > 0.$$

which yields the pointwise optimality condition of Definition 1. \square

Based on the optimality condition (25), [3] suggests to use a fixed point iteration to update the level set function. In Algorithm 1 we present this algorithm adapted to the nonlinear magnetostatic problem including an offline phase for the precomputation of the topological derivative (21). The condition (25) of Lemma 1 is fulfilled if and only if the algorithm has reached a stationary point, i.e. $\psi^{k+1} = \psi^k$. By the line search we guarantee, that this stationary point is indeed a local minimizer of the optimization problem.

Remark 7. Since the generalized topological derivative g is not necessarily continuous, we need an additional step to ensure $\psi_k \in \mathcal{S}, k \geq 0$. We do this by replacing g by the solution \tilde{g} of the PDE

$$\begin{aligned}-\varepsilon \Delta \tilde{g} + \tilde{g} &= g \text{ in } D \\ \nabla \tilde{g} \cdot n &= 0 \text{ on } \partial D.\end{aligned}$$

Algorithm 1 Level Set Algorithm for Topology Optimization by Topological Derivative.

Offline phase

Choose samples $0 = t_1 < t_2 < \dots < t_K = t_{\max}$
for $k = 1, \dots, K$ **do**
 Solve exterior problem (15) for $U = t_k e_0$
 Evaluate $f_{1,k}^{f \rightarrow a}, f_{2,k}^{f \rightarrow a}, f_{1,k}^{a \rightarrow f}, f_{2,k}^{a \rightarrow f}$ (21)
end for
Compute interpolation $\tilde{f}_1^{f \rightarrow a}, \tilde{f}_2^{f \rightarrow a}, \tilde{f}_1^{a \rightarrow f}, \tilde{f}_2^{a \rightarrow f}$ (22)

Online phase

Choose $\psi_0 \in \mathcal{S}, k = 0, k_{\max} < \infty, \varepsilon > 0, 0 < s_{\min} < s_{\max} \leq 1, \gamma \in (0, 1), \delta \geq 1$
Evaluate $\mathcal{J}(\Omega_{\psi_0})$ (evaluate (9) by solving state equation (5))
for $k = 0, \dots, k_{\max}$ **do**
 Compute $g_k = g_{\Omega_{\psi_k}}$ (solve adjoint equation (11), evaluate (22),(20), apply (24))
 if $\theta_k = \arccos \frac{(\psi_k, g_k)_{L_2(D)}}{\|g_k\|_{L_2(D)}} < \varepsilon$ **then**
 break
 end if
 $s = s_{\max}$
 while $s > s_{\min}$ **do**
 $\psi_{k+1} = \frac{1}{\sin \theta_k} \left(\sin((1-s)\theta_k) \psi_k + \sin(s\theta_k) \frac{g_k}{\|g_k\|_{L_2(D)}} \right)$
 if $\mathcal{J}(\Omega_{\psi_{k+1}}) < \mathcal{J}(\Omega_{\psi_k})$ **then** (evaluate (9) by solving (5))
 $s = \min\{s_{\max}, \delta s\}$
 break
 else
 $s = \max\{s_{\min}, \gamma s\}$
 end if
 end while
end for

If D and g are sufficiently regular we get $\tilde{g} \in H^{1+\delta}(D) \hookrightarrow C(D)$ since $D \subset \mathbb{R}^2$. This procedure is similar to sensitivity filtering in density based optimization, the smoothing parameter ε is related to the minimal feature size, see e.g. [35]. The condition $\|\psi_k\|_{L_2(D)} = 1$ is fulfilled by construction of the update step as spherical linear interpolation.

3.3 Robust Optimization

Algorithm 1 is a powerful tool for finding locally optimal topologies under deterministic conditions. However, practical engineering designs - especially in the context of electrical machines - are rarely free from uncertainty. To ensure that solutions remain effective and reliable under such real-world conditions, it is important to incorporate uncertainty into the optimization process. To address these challenges, we now present a general framework for solving a robust optimization problem. As discussed in the introduction in Section 1, uncertainties can arise from both design variables x and model parameters q . In practical applications, uncertainties in model parameters q may arise from measurement errors, model approximations, or environmental conditions and were already introduced as parameter uncertainty. Similarly, uncertainties in design variables x can result from manufacturing tolerances. In optimization without considering uncertainties, the problem is often solved to a high numerical accuracy. However, the precise optimized design cannot be achieved in practice due to limitations in manufacturing and implementation. To handle these uncertainties, we define an uncertainty set $U = U_x \times U_q$ where U_x contains the possible variations of the design variable δx and U_q all possible uncertain values of the parameters q that are in a region around the nominal value $\hat{q} \in U_q$. These sets can be defined using prior knowledge, statistical data, or uncertainty quantification and are fixed since we are using a deterministic approach. Choosing a reasonable region around the nominal value ensures that the robust solution performs well without being overly conservative.

Remark 8. A common choice for the uncertainty sets are closed ellipsoids:

- Uncertainty set for model parameters:

$$U_q = \{q \in \mathbb{R}^{n_q} \mid q = \hat{q} + R_q v_q : v_q \in \mathbb{R}^{n_q}, \|v_q\|_2 \leq 1\},$$

where $\hat{q} \in \mathbb{R}^{n_q}$ is the nominal parameter, and $R_q \in \mathbb{R}^{n_q \times m_q}$ is a matrix with $\text{rank}(R_q) = m_q \leq n_q$ that defines the shape and size of the ellipsoidal uncertainty region in the parameter space.

- Uncertainty set for design variables:

$$U_x = \{\delta x \in \mathbb{R}^{n_x} \mid \delta x = R_x v_x : v_x \in \mathbb{R}^{n_x}, \|v_x\|_2 \leq 1\},$$

where $R_x \in \mathbb{R}^{n_x \times m_x}$ is also a matrix with $\text{rank}(R_x) = m_x \leq n_x$ and characterizes the admissible design perturbations.

We now derive the robust optimization formulation similar to [30, 34] of the nominal problem

$$\min_x g(x, q) \quad (26)$$

with $g : \mathbb{R}^{n_x} \times \mathbb{R}^{n_q} \rightarrow \mathbb{R}$ a real valued function. Incorporating the uncertainties in the design variables $\delta x \in U_x$ and model parameters $q \in U_q$ yields the robust optimization problem

$$\min_x \max_{(\delta x, q) \in U_x \times U_q} g(x + \delta x, q). \quad (27)$$

Next we introduce the worst case function which is the value function of the inner maximization problem

$$f(x) = \max_{(\delta x, q) \in U_x \times U_q} g(x + \delta x, q). \quad (28)$$

Using this, we can rewrite the robust optimization problem (27) as

$$\min_x f(x) \quad (29)$$

Remark 9. In our application g is the reduced cost functional of a PDE constrained optimization problem as introduced in (9).

Remark 10. Solving (27) directly by brute force, i.e. sampling the uncertainty set, is computationally expensive and often intractable. A comprehensive overview of problems of the form (27) can be found in [37]. Some robust optimization problems can be related to bilevel optimization problems. The connections between robust optimization and bilevel optimization are discussed in detail in [26]. To obtain tractability for the inner maximization $(\delta x, q) \mapsto g(x + \delta x, q)$ in (28), g is typically approximated using either a linear [17] or quadratic Taylor expansion [34], where the approximated problem is then solved. However, while a linear approximation provides an analytical solution formula, the approximation quality suffers for highly nonlinear problems. A quadratic approximation offers higher accuracy and leads to a Trust Region problem, but requires up to third-order derivatives, which is very tedious in cases involving PDE constraints.

In this work, we directly address the inner maximization problem and apply a theorem of Clarke on generalized gradients of value functions [13, Thm. 2.1], which under quite general assumptions requires only first-order derivatives [16, 8]. A related approach is used in [8], where descent directions of the worst case functions are used. We rely on the following version of [13, Thm. 2.1], see also [30, Thm. 1].

Theorem 1. *Let $U_x \times U_q \subset \mathbb{R}^{n_x} \times \mathbb{R}^{n_q}$ be convex and compact, and let $g : \mathbb{R}^{n_x} \times U_q \rightarrow \mathbb{R}$ be continuous and continuously differentiable with respect to x . Then the following properties hold for $f(x)$, as defined in (28):*

1. $f(x)$ is locally Lipschitz continuous and directionally differentiable.
2. If $U^*(x)$ denotes the set of maximizers $(\delta x^*, q^*)$ in (28), then Clarke's generalized gradient of $f(x)$ is given by:

$$\partial f(x) = \text{conv} \{ \nabla_x g(x + \delta x^*, q^*) \mid (\delta x^*, q^*) \in U^*(x) \}. \quad (30)$$

3. If $U^*(x)$ contains a single element, then $f(x)$ is differentiable at x , and (30) provides the classical gradient.

Proof. The proof can be found in [13, Thm. 2.1]. □

In summary, this approach has the advantage that only first-order derivatives are required, and with (30) we have a direct formula for computing the subgradient with respect to the worst case function. Compared to solving the robust problem (27) directly, the additional cost is given by finding the worst case of the inner maximization problem, as the outer optimization is similar to the nominal problem (26), but usually nonsmooth. So a crucial step is to determine a maximizer $(\delta x^*, q^*) \in U^*(x)$ to evaluate $f(x)$ and $g \in \partial f(x)$.

Remark 11. A related approach can be found in [11], where Clarke's subdifferential is used to solve robust shape optimization problems of the form (29) with uncertain parameters. In contrast, we focus in this work on topology optimization using the topological derivative.

4 Robust Topology Optimization

In this section we present a combination of the level set based topology optimization using the topological derivative from Section 3.2 and the robust optimization considering the worst case from Section 3.3. Since the set of designs \mathcal{E} is not a normed vector space, uncertainties on the design cannot be considered in a straightforward way by the presented theory. Thus, we restrict ourselves to uncertainties in the additional parameter $q \in U \subset \mathbb{R}^{n_q}$ and do not consider uncertainties in the optimization variable $\Omega \in \mathcal{E}$ (corresponding to $x \in \mathbb{R}^{n_x}$ in (26)). The extension to geometric uncertainties is left open for future research. Our goal is to solve the robust topology optimization problem

$$\min_{\Omega \in \mathcal{E}} \max_{q \in U} \mathcal{J}(\Omega, q), \quad (31)$$

with \mathcal{J} as defined in (9).

4.1 Theoretical result

For a functional $\mathcal{J} : \mathcal{E} \times U \rightarrow \mathbb{R}$ we define the worst case function with respect to q by

$$\varphi(\Omega) := \max_{q \in U} \mathcal{J}(\Omega, q). \quad (32)$$

In order to show the main theoretical result we need the following assumption.

Assumption 1. Let $\mathcal{J} : \mathcal{E} \rightarrow \mathbb{R}$ be a real-valued shape function. We assume that there exists a $\tau_0 > 0$ such that the mapping

$$\tau \mapsto \frac{1}{|\omega|} \mathcal{J}(\Omega_{\sqrt{\tau}}(z)) \quad (33)$$

is continuously differentiable for all $\tau \in [0, \tau_0]$ and all $z \in \Omega$ with $\Omega_\epsilon(z)$ and $\omega_\epsilon(z) = \epsilon\omega + z$, $\omega = B_1(0)$ as in (12).

We now show that this assumption implies the existence of the topological derivative of $\Omega \mapsto \mathcal{J}(\Omega)$

Lemma 2. *Let $\mathcal{J} : \mathcal{E} \times U \rightarrow \mathbb{R}$ be a real valued function. Assume that Assumption 1 holds for $\mathcal{J}(\cdot, q)$, for all $q \in U$. Then, for $z \in \Omega$, the function*

$$\tau \mapsto \tilde{g}(\tau, q) = \frac{1}{|\omega|} \mathcal{J}(\Omega_{\sqrt{\tau}}(z), q) \quad (34)$$

is continuously differentiable with respect to τ and the derivative in 0 coincides with the topological derivative

$$\frac{\partial^+}{\partial \tau} \tilde{g}(0, q) = \frac{\partial}{\partial \Omega} \mathcal{J}(\Omega, q) := \lim_{\epsilon \searrow 0} \frac{\mathcal{J}(\Omega_\epsilon(z), q) - \mathcal{J}(\Omega, q)}{|\omega_\epsilon(z)|} \quad (35)$$

for all $q \in U$.

Proof. Let $z \in \Omega, q \in U$ be arbitrary but fixed. The partial differentiability of \tilde{g} follows by assumption. We conclude

$$\frac{\partial^+}{\partial \tau} \tilde{g}(0, q) = \lim_{\delta \searrow 0} \frac{\tilde{g}(\delta, q) - \tilde{g}(0, q)}{\delta} \stackrel{\delta = \epsilon^2}{=} \lim_{\epsilon \searrow 0} \frac{\mathcal{J}(\Omega_\epsilon(z)) - \mathcal{J}(\Omega)}{|\omega| \epsilon^2}, \quad (36)$$

which gives the desired identification. \square

We now prove that the topological derivative of the worst case objective function exists and can be written in a simple form using Theorem 1 which is based on [13, Thm 2.1].

Theorem 2. Let $U \subset \mathbb{R}^{n_q}$ be a convex compact set and $\mathcal{J} : \mathcal{E} \times U \rightarrow \mathbb{R}$ be a real valued objective function. We assume that, for all $q \in U$, Assumption 1 holds for $\mathcal{J}(\cdot, q)$. Furthermore we assume that the set of maximizers $U^*(\Omega)$ of the mapping $q \mapsto \mathcal{J}(\Omega, q)$ is a singleton and define the worst case parameter

$$q^*(\Omega) := \arg \max_{q \in U} \mathcal{J}(\Omega, q), \quad (37)$$

for $\Omega \in \mathcal{E}$. Then the topological derivative of the worst case function (32), $\frac{d}{d\Omega} \varphi(\Omega)$, exists for $z \in \Omega$ and is given by:

$$\frac{d}{d\Omega} \varphi(\Omega)(z) = \frac{\partial}{\partial \Omega} \mathcal{J}(\Omega, q^*(\Omega)). \quad (38)$$

Proof. By Lemma 2, the function $\tau \mapsto \tilde{g}(\tau, q)$, defined in (34), is continuously differentiable on $[0, \tau_0]$ for $q \in U$. This yields the existence of a partially continuously differentiable extension $g : \mathbb{R} \times U \rightarrow \mathbb{R}$ with

$$g(\tau, q) = \tilde{g}(\tau, q) = \frac{1}{|\omega|} \mathcal{J}(\Omega_{\sqrt{\tau}}, q),$$

for $\tau \in [0, \tau_0], q \in U$. For g we define the worst case function $f : \mathbb{R} \rightarrow \mathbb{R}$,

$$f(\tau) := \max_{q \in U} g(\tau, q).$$

Note, that for $\tau \in [0, \tau_0]$ the worst cases of g and \mathcal{J} coincide

$$q^*(\tau) := \arg \max_{q \in U} g(\tau, q) = \arg \max_{q \in U} \mathcal{J}(\Omega_{\sqrt{\tau}}, q) = q^*(\Omega_{\sqrt{\tau}}).$$

Similarly we can identify the worst case functions for $\tau \in [0, \tau_0]$

$$f(\tau) = g(\tau, q^*(\tau)) = \frac{1}{|\omega|} \mathcal{J}(\Omega_{\sqrt{\tau}}, q^*(\Omega_{\sqrt{\tau}})) = \frac{1}{|\omega|} \varphi(\Omega_{\sqrt{\tau}}).$$

We apply Theorem 1 to the function $g : \mathbb{R} \times U \rightarrow \mathbb{R}$ and get that the derivative of f exists in 0 and can be computed as follows:

$$\frac{d}{d\tau} f(0) = \frac{\partial}{\partial \tau} g(0, q^*(0)) = \frac{\partial^+}{\partial \tau} \tilde{g}(0, q^*(0)). \quad (39)$$

Plugging in the definition of f we get

$$\frac{d}{d\Omega} \varphi(\Omega)(z) = \lim_{\epsilon \searrow 0} \frac{\varphi(\Omega_\epsilon(z)) - \varphi(\Omega)}{|\omega_\epsilon(z)|} \stackrel{\tau=\epsilon^2}{=} \lim_{\tau \searrow 0} \frac{f(\tau) - f(0)}{\tau} = \frac{d}{d\tau} f(0)$$

which, together with (39) and (36), gives the desired result. \square

Theorem 2 states that, under the given assumptions, the robust topological derivative, i.e. the topological derivative of the worst case function φ is given by evaluating the topological derivative of the nominal problem at the worst case parameter $q^*(\Omega)$. This leads to a natural extension of the level set algorithm to robust topology optimization problems.

Corollary 1. *Let $\varphi(\Omega) := \max_{q \in U} \mathcal{J}(\Omega, q)$ bet the worst case function of the robust design optimization problem (31) with a linear PDE constraint, i.e. with a linear material law $h_f(b) = \nu_f b$ in (5). Assume that the set of maximizers $U^*(\Omega) := \{q^* \in U : \mathcal{J}(\Omega, q^*) = \varphi(\Omega)\}$ is a singleton for all $\Omega \in \mathcal{E}$. Then φ is topologically differentiable for $z \in \Omega$ with*

$$\frac{d}{d\Omega} \varphi(\Omega)(z) = \frac{\partial}{\partial \Omega} \mathcal{J}(\Omega, q^*(\Omega)).$$

Proof. Assumption 1 for $\mathcal{J}(\cdot, q)$ is shown in Lemma 3 in the Appendix. Theorem 2 yields the desired result \square

Remark 12. For the more general case of a nonlinear relation $h_f = f(b)$ which is usually used in electric machine simulation, a result corresponding to Lemma 3 is currently not available in the literature. This is subject of ongoing and future research.

Remark 13. Of course assuming the uniqueness of the worst case $q^*(\Omega)$ is a strong assumption. However Theorem 1 states that if the set of maximizers $U^*(x)$ is not a singleton one should continue with an element of the convex hull of derivatives for all elements of $U^*(x)$. In particular, taking the gradient evaluated in one element of $U^*(x)$ is valid. We will follow this approach in the numerical realization by choosing the element we obtain by numerically maximizing $q \mapsto \mathcal{J}(\Omega, q)$ using Algorithm 2 as $q^*(\Omega)$.

4.2 Numerical Algorithm

We define the generalized robust topological derivative for $z \in \Omega$ by

$$g_{\Omega, q}(z) = \begin{cases} \frac{d^{f \rightarrow a}}{d\Omega} \mathcal{J}(\Omega, q^*(\Omega))(z) & \text{if } z \in \Omega_f \\ -\frac{d^{a \rightarrow f}}{d\Omega} \mathcal{J}(\Omega, q^*(\Omega))(z) & \text{if } z \in \Omega_a. \end{cases} \quad (40)$$

Adding the computation of the worst case q^* to the level set algorithm Algorithm 1, we arrive at the robust counterpart sketched in Algorithm 3. To determine the worst case $q^*(\Omega)$ we solve the constrained maximization problem by a projected gradient method stated in Algorithm 2. The operator \mathcal{P}_U denotes the orthogonal projection onto the uncertainty set U and the gradient $\nabla_q \mathcal{J}$ is computed by

$$\nabla_q \mathcal{J}(\Omega, q) = \nabla_q \mathcal{G}(\Omega, q, (\alpha^1, \dots, \alpha^N), (u^1, \dots, u^n, \lambda^1, \dots, \lambda^n), (p^1, \dots, p^n, \eta^1, \dots, \eta^n))$$

Algorithm 2 Parameter Optimization Algorithm of the Inner Problem.

Choose $q^0 \in U, l_{\max} < \infty, \varepsilon_\tau > 0, 0 < \tau_{\min} < \tau_{\max} < \infty, \gamma_\tau \in (0, 1), \delta_\tau \geq 1, \gamma \in (0, \frac{1}{2})$
Evaluate $\mathcal{J}(\Omega, q^0)$ (evaluate (9) by solving state equation (5))
for $l = 0, \dots, l_{\max}$ **do**
 Compute $\nabla_q \mathcal{J}(\Omega, q^l)$ (solve adjoint equation (11), evaluate (41))
 $\tau = \tau_{\max}$
 while $\tau > \tau_{\min}$ **do**
 $q^{l+1} = \mathcal{P}_U(q^l + \tau \nabla_q \mathcal{J}(\Omega, q^l))$
 if $\mathcal{J}(\Omega, q^{l+1}) - \mathcal{J}(\Omega, q^l) \geq \gamma/\tau \|q^{l+1} - q^l\|^2$ **then** (solve (5), evaluate (9))
 $\tau = \min\{\tau_{\max}, \delta_\tau \tau\}$
 break
 else
 $\tau = \max\{\tau_{\min}, \gamma_\tau \tau\}$
 end if
 end while
 if $\|q^{l+1} - q^l\| < \varepsilon_\tau$ **then**
 break
 end if
end for

where \mathcal{G} is the Lagrangian defined in (10), (u^n, λ^n) solves the state equation (5) and (p^n, η^n) the adjoint equation (11) for $n = 0, \dots, N - 1$.

Remark 14. Let us state this expression for the specific uncertainties which we are considering. Both are incorporated via the PDE constraint (5). We consider uncertainties in the source current $j(\alpha, q)$ and the material law $h_\Omega(b, q)$. The gradient of \mathcal{J} is then computed by

$$\nabla_q \mathcal{J}(\Omega, q) = \sum_{n=0}^{N-1} \int_{D_{\text{all}}} \nabla_q h_\Omega(\text{curl} u^n, q) \cdot \text{curl} p^n \, dx - \int_{D_{\text{all}}} \nabla_q j(\alpha^n, q) p^n \, dx. \quad (41)$$

Remark 15. In order to apply Theorem 2 it is necessary that $q^*(\Omega)$ is indeed a global maximizer. We try to guarantee this by choosing the initial guess q^0 wisely, because the quality of the solution of the local maximization problems depends on the starting point q^0 . If $U = [u_1, u_2] \subset \mathbb{R}$ is an interval, we use $q^0 \in \{u_1, u_2\}$, the boundary points of U , as initial guesses for the inner maximization problem. This approach is motivated by the observation that promising candidates for the maximizer q^* for such physical problems often lie on the boundary of U . However, care must be taken if $U \subset \mathbb{R}^n$, as selecting an inappropriate boundary point may lead to suboptimal solutions and fail to identify the worst case. For further details we refer the interested reader to [6].

Algorithm 3 Robust Topology Optimization Algorithm with Level Set and Topological Derivative.

Offline phase

Choose samples $0 = t_1 < t_2 < \dots < t_K = t_{\max}, q_1, \dots, q_L \in U$
for $l = 1, \dots, L$ **do**
 for $k = 1, \dots, K$ **do**
 Solve exterior problem (15) for $U = t_k e_0, q = q_l$
 Evaluate $f_{1,l,k}^{f \rightarrow a}, f_{2,l,k}^{f \rightarrow a}, f_{1,l,k}^{a \rightarrow f}, f_{2,l,k}^{a \rightarrow f}$ considering $h = h(b, q_l)$ (21)
 end for
end for
Compute interpolation $\tilde{f}_1^{f \rightarrow a}, \tilde{f}_2^{f \rightarrow a}, \tilde{f}_1^{a \rightarrow f}, \tilde{f}_2^{a \rightarrow f}$ (22)

Online phase

Choose $\psi_0 \in \mathcal{S}, k_{\max} < \infty, \varepsilon > 0, 0 < s_{\min} < s_{\max} \leq 1, \gamma \in (0, 1), \delta \geq 1$
for $k = 0, \dots, k_{\max}$ **do**
 Find q_k^* by Algorithm 2 for $\Omega = \Omega_{\psi_k}$
 Compute $g_k = g_{\Omega_{\psi_k}, q_k^*}$ (solve adjoint equation (11), evaluate (20)(22) considering q_k^* , apply (40))
 if $\theta_k = \arccos \frac{(\psi_k, g_k)_{L_2(D)}}{\|g_k\|_{L_2(D)}} < \varepsilon$ **then**
 break
 end if
 $s = s_{\max}$
 while $s > s_{\min}$ **do**
 $\psi_{k+1} = \frac{1}{\sin \theta_k} \left(\sin((1-s)\theta_k) \psi_k + \sin(s\theta_k) \frac{g_k}{\|g_k\|_{L_2(D)}} \right)$
 Find q_{k+1}^* by Algorithm 2 for $\Omega = \Omega_{\psi_{k+1}}$
 if $\mathcal{J}(\Omega_{\psi_{k+1}}, q_{k+1}^*) < \mathcal{J}(\Omega_{\psi_k}, q_k^*)$ **then** (evaluate (9) by solving (5))
 $s = \min\{s_{\max}, \delta s\}$
 break
 else
 $s = \max\{s_{\min}, \gamma s\}$
 end if
 end while
end for

Remark 16. If the uncertain parameter q affects the material law $h_\Omega(b, q)$ we have to precompute the topological derivative (21) also for samples $q_0, \dots, q_L \in U$. This is done in the offline phase of Algorithm 3. Depending on its dimension this can get computationally costly. However, since these precomputations are independent of each other one can do this in parallel. If q acts only on j this is not necessary and the loop over $l = 0, \dots, L$ in the offline phase of Algorithm 3 can be skipped.

Remark 17. Compared to the non-robust optimization algorithm we have to additionally solve the inner maximization problem which is computationally costly. The computational overhead depends on the initial guesses and the regularity with respect to the parameter. In Section 5 we present a comparison of computation time for nominal and robust optimization for our applications, see Table 4.

5 Numerical Results

In this section we present results of the robust design optimization problem (31) applied to an electric machine with uncertainty either in the application current or the material law. In the latter case we distinguish between a scalar parameter or a spatially distributed one. We compare design and worst case values with those obtained by a nominal optimization. An overview of the obtained performances is given in Table 3. We want to point out that our approach is quite general and can be applied not only to electric machines, but to many other engineering problems.

5.1 Implementation and Parameters

In our simulations, we consider (5) with the piecewise defined material law (4) based on the following nominal material laws

$$\begin{aligned} h_a(b) &= \nu_0 b, \\ h_{m_i}(b) &= \nu_m (b - b_R e_{\varphi_i}), i = 1, 2, \\ h_f(b) &= \nu_0 b + (\nu_f - \nu_0) \frac{K_f}{\sqrt[N_f]{K_f^{N_f} + |b|^{N_f}}} b \end{aligned} \tag{42}$$

and a source current density

$$\begin{aligned} j_A(\alpha) &= \hat{j} \sin(4\alpha + \phi_0) \\ j_B(\alpha) &= \hat{j} \sin(4\alpha + \frac{2\pi}{3} + \phi_0) \\ j_C(\alpha) &= \hat{j} \sin(4\alpha + \frac{4\pi}{3} + \phi_0) \end{aligned} \tag{43}$$

ν_0	ν_f	K_f	N_f	ν_m	b_R	φ_1	φ_2	\hat{j}	ϕ_0
$\frac{10^7}{4\pi}$	200	2.2T	12	$\frac{\nu_0}{1.086}$	1.216T	30°	15°	$23.7 \times 10^6 \frac{\text{A}}{\text{m}^2}$	6°

Table 1: Material parameters.

t_{\max}	K	L	ε	s_{\min}	s_{\max}	γ, γ_τ	δ, δ_τ	ε_τ	τ_{\min}	τ_{\max}
5	50	10	2°	0.05	1	0.5	1.5	10^{-3}	10^{-3}	1

Table 2: Parameter values for Algorithm 1, 2, 3.

with parameters given in Table 1. To solve the occurring PDEs (5),(15) we used the open source finite element package NGSolve [45]. Similarly as in [3] we used lowest order finite elements on a triangular mesh with 3995 nodes to solve the state (5) and adjoint equation (11) as well as to represent the level set function (23). The goal is to minimize the negative average torque (9) for $N = 11$ rotor positions (7). To compute the topological derivative (16), which includes solving the auxiliary problem (15), we truncated the unbounded domain \mathbb{R}^2 to a ball with radius 128 and used lowest order finite elements on a triangular mesh with 61272 nodes. The nominal optimization was done using Algorithm 1, for the robust optimization we used Algorithms 2, 3. The parameters in the level set algorithms were chosen as presented in Table 2. The samples in the offline phase of Algorithm 1 are computed for uniformly distributed $0 = t_1 < \dots < t_K = t_{\max}$. If the uncertainty q enters the material law as considered in Section 5.4, we additionally need $q_1, \dots, q_L \in U$ in the offline phase of Algorithm 3, which we also chose uniformly distributed.

5.2 Nominal Optimization

We apply Algorithm 1 to find a solution to the optimization problem without uncertainty (8). After 29 iterations, the level set algorithm converged and we obtained the design Ω_{NOM} shown in Figure 4 with a negative average torque of $\mathcal{J}(\Omega_{\text{NOM}}) = -835\text{Nm}$.

5.3 Uncertain Load Angle

As a first application of the developed robust design optimization algorithm we add uncertainty to the source current density (43), which is the right hand side

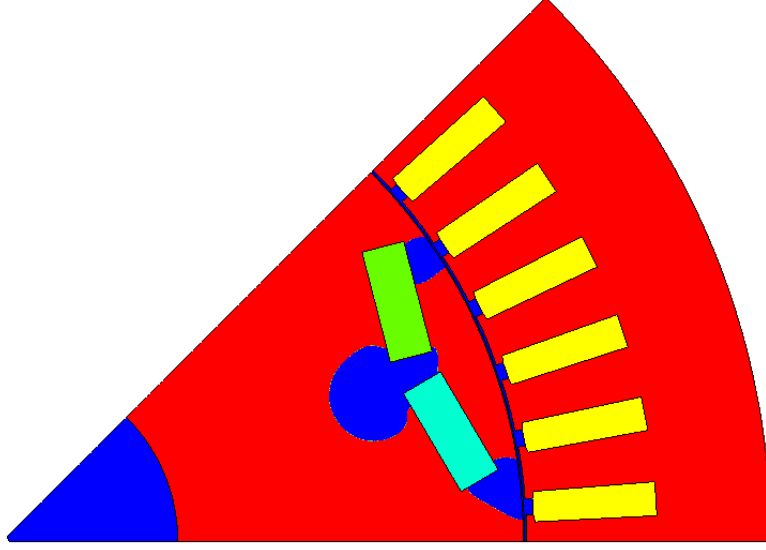


Figure 4: Final design of nominal optimization Ω_{NOM} , $\mathcal{J}(\Omega_{\text{NOM}}) = -835\text{Nm}$.

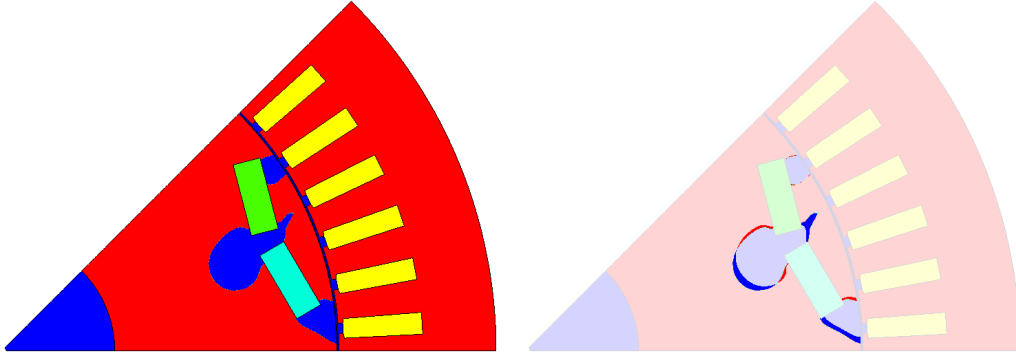


Figure 5: Final design Ω_{ANG} (left), difference from nominal result Ω_{NOM} (right) considering an uncertain load angle, see Section 5.3.

of the magnetostatic PDE (5),

$$\begin{aligned} j_A(\alpha, q) &= \hat{j} \sin(4\alpha + q) \\ j_B(\alpha, q) &= \hat{j} \sin(4\alpha + \frac{2\pi}{3} + q) \\ j_C(\alpha, q) &= \hat{j} \sin(4\alpha + \frac{4\pi}{3} + q), \end{aligned}$$

where q changes the phasing of the electric source current density with respect to the mechanical rotor position α . This parameter is called the load angle. The uncertainty set is chosen as $U = [-9^\circ, 21^\circ]$ with nominal value $\hat{q} = 6^\circ$.

In Figure 5 we present the robustly optimized design Ω_{ANG} obtained after 76 iterations of Algorithm 3 and the difference to the nominally optimized one, i.e.

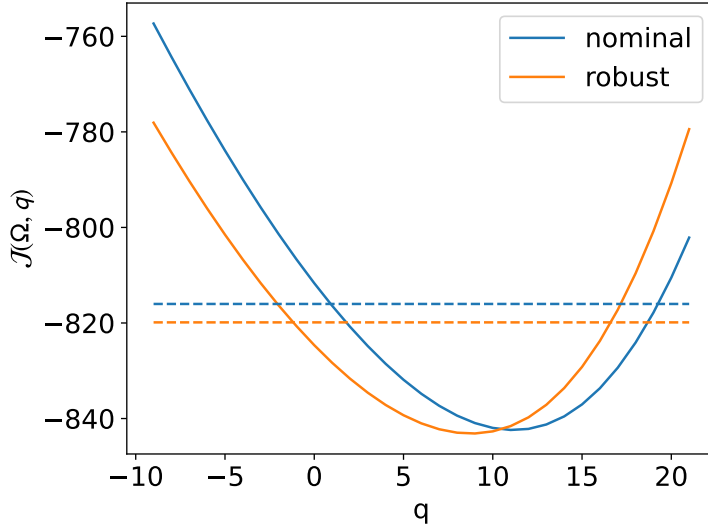


Figure 6: Negative average torque in dependence of $q \in U$ for nominally (blue) and robustly (orange) optimized design with corresponding averages over U (dashed) as considered in Section 5.3.

with $\hat{q} = 6^\circ$. The plot of the performance in dependence of $q \in U$ shows that the worst cases are attained at $q^* = -9^\circ$ for both designs with worst case values $\mathcal{J}(\Omega_{\text{NOM}}, q^*(\Omega_{\text{NOM}})) = -757\text{Nm}$, $\mathcal{J}(\Omega_{\text{ANG}}, q^*(\Omega_{\text{ANG}})) = -778\text{Nm}$. This is an improvement of 3%. Also the nominal value is slightly improved from $\mathcal{J}(\Omega_{\text{NOM}}, \hat{q}) = -835\text{Nm}$ to $\mathcal{J}(\Omega_{\text{ANG}}, \hat{q}) = -841\text{Nm}$ which is 0.7% as well as the average performance over the uncertainty set U from -816Nm to -820Nm . By considering the robustness, we obtained a better local minimizer also for the nominal case. This can be explained by a flattening of the objective, as illustrated in the introductory example Figure 1.

Remark 18. We mention that, in this case, the optimality criterion (25) was not reached. In fact, the algorithm fell into a cyclic behavior of three designs after approximately 60 iterations. We stopped the algorithm after $k_{\text{max}} = 100$ iterations and selected the best performing design.

5.4 Uncertain Material Parameter

We consider an uncertainty in the material law of iron. Using the model (42) we model an uncertain saturation behavior by

$$h_f(b, q) = \nu_0 b + (\nu_f - \nu_0) \frac{q}{\sqrt[N_f]{q^{N_f} + |b|^{N_f}}} b,$$

with $q \in U = [1.76, 2.64]$ which corresponds to a $\pm 20\%$ uncertainty of the nominal value $\hat{q} = K_f = 2.2$, displayed in Figure 7.

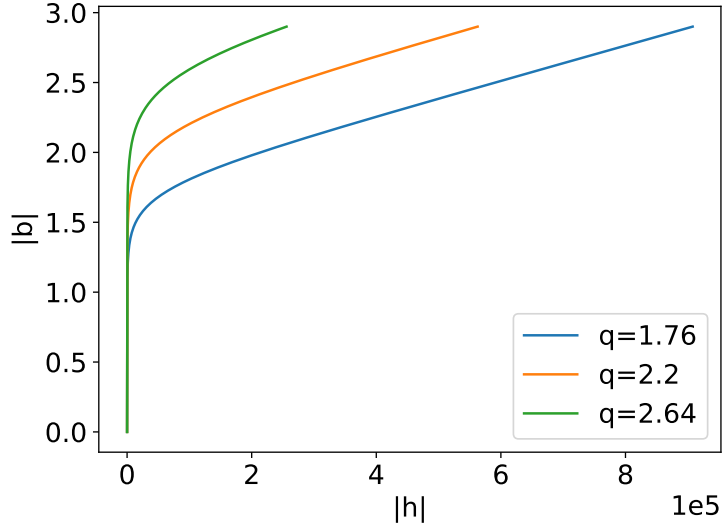


Figure 7: Iron material law for $q \in \{1.76, 2.2, 2.64\}$.

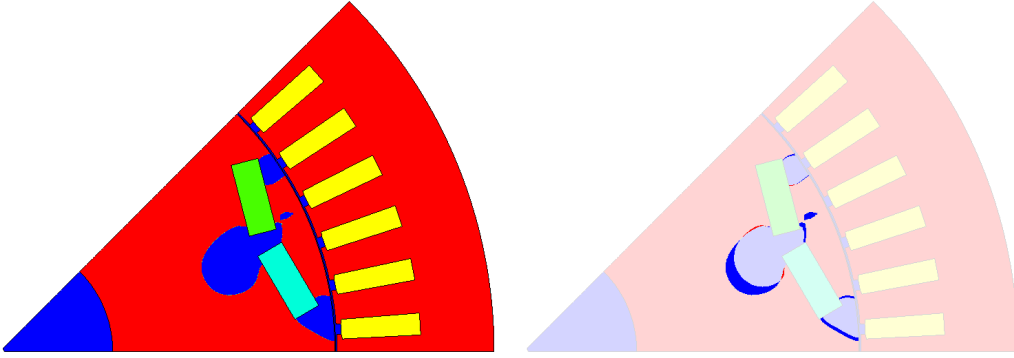


Figure 8: Final design Ω_{SCAL} of robust optimization with uncertain scalar material parameter (left) and difference from the nominal result Ω_{NOM} (right) considering a scalar material uncertainty, see Section 5.4.1.

5.4.1 Scalar Parameter

First we assume that the uncertainty is homogeneous for all iron parts modeled. This corresponds to a scalar parameter $q \in U$. The robust design optimization using Algorithm 3 converged after 30 iterations. The resulting design Ω_{SCAL} is presented in Figure 8. The worst case value of the cost function decreases from $\mathcal{J}(\Omega_{\text{NOM}}, q^*(\Omega_{\text{NOM}})) = -696\text{Nm}$ to $\mathcal{J}(\Omega_{\text{SCAL}}, q^*(\Omega_{\text{SCAL}})) = -701\text{Nm}$ corresponding to an improvement by 0.7%. In Figure 9 one can see that the worst case parameter is $q^* = 1.76$ for both the nominally and the robustly optimized design. The value at the nominal parameter $\hat{q} = 2.2$ is slightly improved from $\mathcal{J}(\Omega_{\text{NOM}}, \hat{q}) = -826\text{Nm}$ to $\mathcal{J}(\Omega_{\text{SCAL}}, \hat{q}) = -829\text{Nm}$.

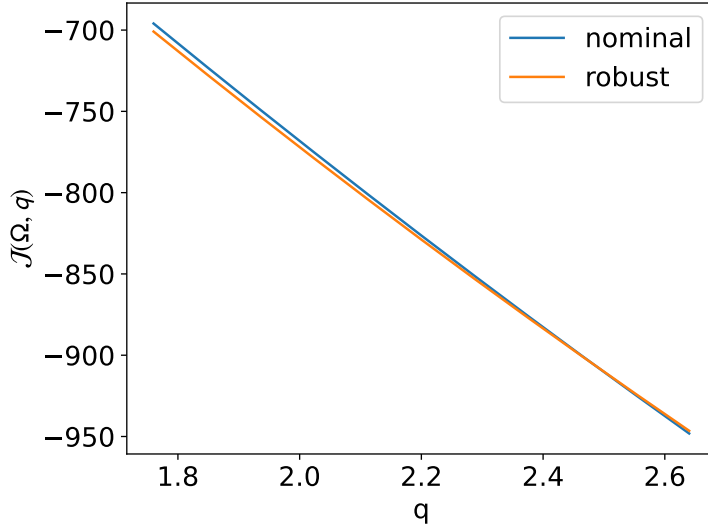


Figure 9: Negative average torque in dependence of $q \in U$ for nominally (blue) and robustly (orange) optimized design, as considered in Section 5.4.1.

5.4.2 Distributed Parameter

We now assume that the uncertainty of the iron material behavior varies spatially. We model this by a parameter function $q : D_{\text{all}} \rightarrow U$ with uncertain values in U . The robustly optimized design Ω_{DIST} is shown in Figure 10 (left) together with the difference from the nominally optimized design Ω_{NOM} (right). Here, Algorithm 3 converged after 23 iterations. The worst case function values give a small improvement from $\mathcal{J}(\Omega_{\text{NOM}}, q^*(\Omega_{\text{NOM}})) = -692\text{Nm}$ to $\mathcal{J}(\Omega_{\text{DIST}}, q^*(\Omega_{\text{DIST}})) = -696\text{Nm}$. In Figure 11 we display the spatial distribution of the worst case parameter functions $q^*(\Omega_{\text{DIST}})$, $q^*(\Omega_{\text{NOM}})$ for the robustly and nominally optimized designs, respectively, which are barely different. We observe that q^* attains only values on the boundaries of $U = [1.76, 2.64]$. Since the lower value 1.76 highly dominates, which was also the worst case in the previous optimization in Section 5.4.1, it is feasible that the resulting designs and torque values are very close to each other, see Figure 8 and Figure 10. In Table 3 we compare the worst case function values for the nominally and robustly optimized designs.

Remark 19. In Figure 11 we observe a very homogeneous worst case parameter distribution in the stator D_S compared to the rotor D_R . One can give an engineering explanation for this phenomenon: The occurring magnetic fields, coming from the permanent magnets and the excitation current, move with the same speed as the rotor. Therefore the rotor has an almost static field with small oscillations. On the other hand, the pointwise temporal average of the field in the stator is zero. Since we consider the average torque, a possible spatial variation of the uncertainty in the stator is canceled.

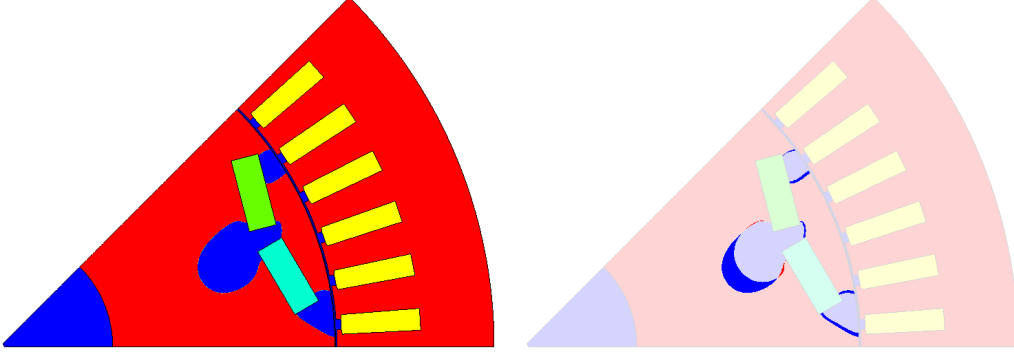


Figure 10: Final design Ω_{DIST} for robust optimization (left), difference from the nominal result Ω_{NOM} (right) considering a distributed material uncertainty, see Section 5.4.2.

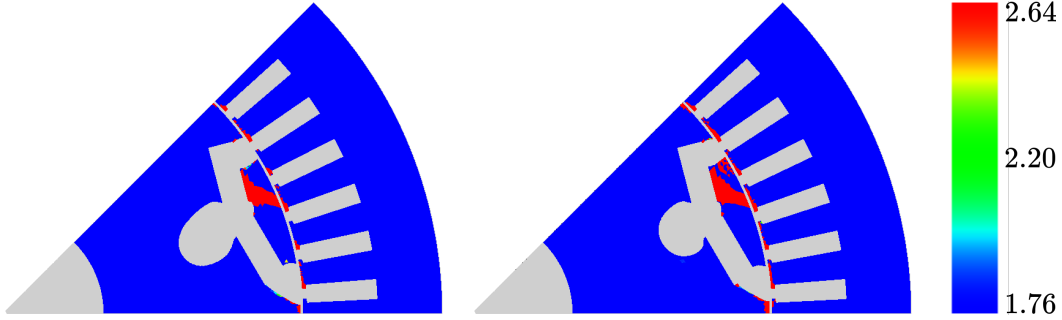


Figure 11: Worst case parameter function for final designs, $q^*(\Omega_{\text{DIST}})$ (left), $q^*(\Omega_{\text{NOM}})$ (right) considering a distributed material uncertainty, see Section 5.4.2.

Remark 20. When computing the topological derivative $\frac{d^{a \rightarrow f}}{d\Omega} \mathcal{J}(\Omega, q)(z)$ for $z \in \Omega_a$ one has to assign a value for $q(z)$ in the iron perturbation. This issue is often encountered in combined design and parameter optimization. The presence of air hides the effect of q in Ω_a . In this case we decided to set q^* to the nominal value $q^* = q^* \chi_{\Omega_f} + 2.2 \chi_{\Omega_a}$.

Remark 21. Since the spatially distributed uncertainty results in an inhomogeneous material behavior, we have to be careful when using symmetries of the machine geometry. Since every pole (in our case a piece of 45°) has the same contribution to the torque it is feasible that the worst case q^* is also the same for each pole. However, to get the correct average torque we have to simulate a mechanical rotation over a full pole (different to the previous cases, where it was sufficient to consider a third of a pole, see (7)). We did so by taking $N = 33$ uniform angular positions $\alpha^0, \dots, \alpha^{N-1}$ within 45° .

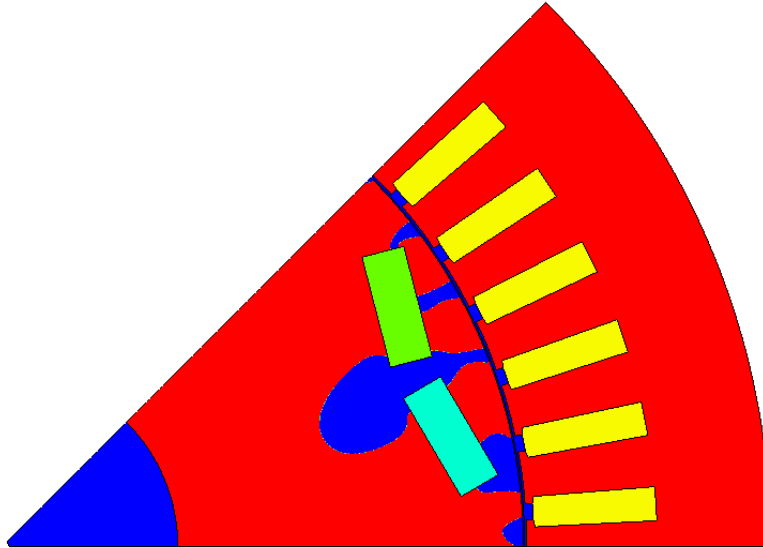


Figure 12: Final design Ω_{NOM1} for nominal optimization considering a single rotor position, see Section 5.4.3.

Name	Nominal [Nm]	Robust [Nm]
ANG	-757	-778
SCAL	-696	-701
DIST	-692	-696
DIST1	-870	-989

Table 3: Overview of worst case function values for different applications: Uncertain load angle (ANG), see Section 5.3; uncertain scalar material parameter (SCAL), see Section 5.4.1; uncertain distributed material parameter for average torque (DIST), see Section 5.4.2; single rotor position (DIST1), see Section 5.4.3.

5.4.3 Single Rotor Position

To highlight the effect of robust optimization we consider the torque for a single rotor position choosing $N = 1$ in (8). We obtain a new result of the nominal optimization Ω_{NOM1} presented in Figure 12. The corresponding worst case parameter distribution $q^*(\Omega_{\text{NOM1}})$ (Figure 14, left) is very different to the previous one (Figure 11, left) from Section 5.4.2, where we considered the average torque. The robust optimization using Algorithm 3 results in a slightly different design Ω_{DIST1} , shown in Figure 13, with worst case function $q^*(\Omega_{\text{DIST1}})$ displayed in Figure 14 (right). We see a significant change in the worst case function which yields a high performance improvement from $\mathcal{J}(\Omega_{\text{NOM1}}, q^*(\Omega_{\text{NOM1}})) = -870\text{Nm}$ to $\mathcal{J}(\Omega_{\text{DIST1}}, q^*(\Omega_{\text{DIST1}})) = -989\text{Nm}$ which is 13.7%.

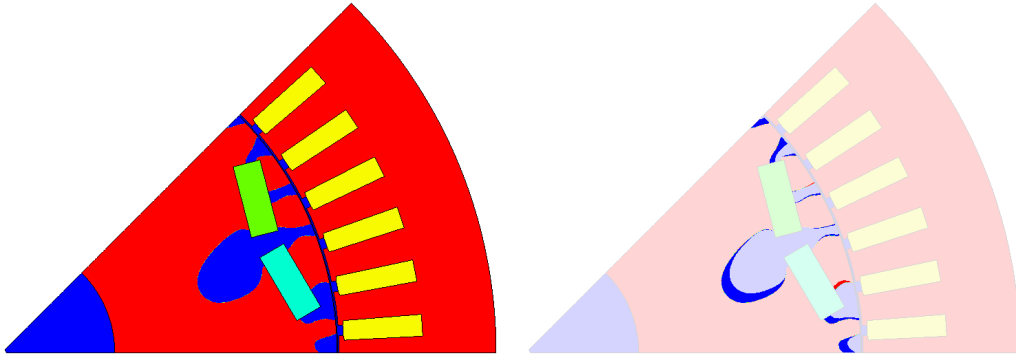


Figure 13: Final design Ω_{DIST1} for nominal optimization (left), difference from the nominal result Ω_{NOM1} (right) considering a distributed material uncertainty and a single rotor position, see Section 5.4.3.

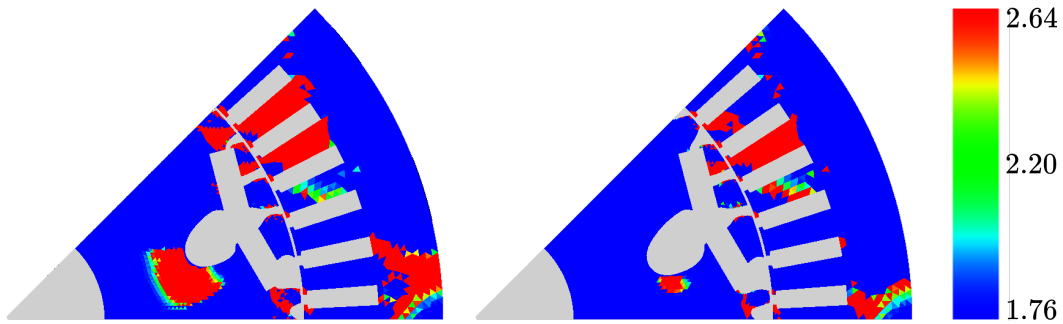


Figure 14: Worst case parameter functions for final designs, $q^*(\Omega_{\text{NOM1}})$ (left), $q^*(\Omega_{\text{DIST1}})$ (right) considering a distributed material uncertainty and a single rotor position, see Section 5.4.3.

Name	Iterations	Function evaluations	Gradient evaluations	Rotor positions	Time [s]	Factor to nominal
NOM	29	46	29	11	620	1
ANG	76	513	203	11	4628	7.5
SCAL	30	165	71	11	1332	2.1
DIST	23	763	304	33	16428	26.5
NOM1	65	88	65	1	111	1
DIST1	67	1973	796	1	1324	11.9

Table 4: Overview of computational effort for different design optimizations: Nominal optimization (NOM), see Section 5.2, robust optimization with uncertain load angle (ANG), see Section 5.3; uncertain scalar material parameter (SCAL), see Section 5.4.1; uncertain distributed material parameter for torque (DIST), see Section 5.4.2; nominal optimization for single rotor position (NOM1), see Section 5.4.3; robust optimization with distributed material uncertainty for single rotor position (DIST1), see Section 5.4.3.

5.5 Computation Time

All computations were done using a single Intel i5 core with 2.4GHz. We present an overview of the optimization for all examples in Table 4. We see that for the nominal optimizations we performed one gradient evaluation per iteration. Due to the line search we needed more than one function evaluation per iteration for all cases. The algorithm converged slower in terms of number of iterations for the optimizations where we considered a single rotor position (NOM1, DIST1). This indicates that considering the average torque has a smoothing effect on the design optimization problem. In the last column of Table 4 we present the cost of the robust optimization relative to the nominal optimization. The computational overhead of the robust optimizations comes from the evaluation of the worst case function which includes solving the inner maximization problem. The robust optimizations were between 2.1 and 11.9 times slower than the nominal optimizations, except in the case where we optimized the average torque considering a distributed material uncertainty (DIST). If we account for the fact that due to physical reasons we had to consider more rotor positions we may scale the computation time for this case and result at an overhead factor $26.5/3 = 8.8$ which is in the range of the other robust optimizations.

6 Conclusion and Future Work

This paper presented a novel and efficient method for robust design optimization of electric machines, combining the topological derivative and a level set-based approach with a robust optimization framework. The method efficiently solves

min-max problems to find designs that are robust against material uncertainties. The proposed approach was applied to a two-material robust topology optimization of a PMSM machine, demonstrating improved worst case performance with minimal trade-offs in nominal performance. Although the parameters load angle and material saturation were used, any parameter can be selected to be robustified. The results highlight the potential of robust topology optimization for designing reliable and efficient electric machines. We have proven theoretical results for linear PDE constraints. However, the method has also turned out to be effective in the more general case of quasilinear PDEs. A theoretical justification for this generalization is the subject of ongoing research. Future work could focus on several promising extensions of this framework. One direction is to incorporate the geometric uncertainty through the level set function, which would represent the manufacturing tolerances due to a production process. In addition, the approach could be applied to other engineering problems with complex design requirements, demonstrating its application across disciplines. Finally, uncertainty quantification techniques could be used to model more realistic and data-driven uncertainty sets, making them more applicable to industry.

A Appendix

The following lemma is based on results presented in [40] where the topological derivative for a linear diffusion problem is obtained as a limit of the shape derivative with respect to the variation of a circular hole as the hole's radius tends to zero. We use these results to show that Assumption 1 is satisfied in the case of linear material behavior.

Lemma 3. *Let $\mathcal{J} : \mathcal{E} \rightarrow \mathbb{R}$ be the reduced cost function of the nominal problem (9) with a linear PDE constraint, i.e. $h_f(b) = \nu_f b$ in (5). Then Assumption 1 holds true.*

Proof. We will use the shape derivative according to [48]. A shape function $\mathcal{J} : \mathcal{E} \rightarrow \mathbb{R}$ is said to be shape differentiable if the limit

$$d^S \mathcal{J}(\Omega)(V) := \lim_{t \rightarrow 0} \frac{\mathcal{J}((\text{id} + tV)(\Omega)) - \mathcal{J}(\Omega)}{t} \quad (44)$$

exists for all $V \in C_c^\infty(D)^2$ in \mathbb{R} , where id is the identity map, and the map $V \mapsto d^S \mathcal{J}(\Omega)(V)$ is linear and continuous with respect to the topology of $C_c^\infty(D)^2$. We call $d^S \mathcal{J}(\Omega)$ the shape derivative of \mathcal{J} . For $z \in \Omega$, $\epsilon > 0$ we define a smooth vector field $V_\epsilon^{\text{rad}}(z) \in C_c^\infty(D)^2$ which coincides on the boundary of the perturbation $\omega_\epsilon(z)$ with the outer unit normal vector

$$V_\epsilon^{\text{rad}}(z)|_{\partial\omega_\epsilon} = \frac{x - z}{\epsilon}. \quad (45)$$

As mentioned in Remark 1 we can rewrite the constraining PDE (5) as a linear diffusion equation. For problems of this kind, the identity from [40, Prop. 1.1]

$$\frac{d}{d\Omega} \mathcal{J}(\Omega)(z) = \lim_{\epsilon \searrow 0} \frac{1}{2|\omega|\epsilon} d^S \mathcal{J}(\Omega_\epsilon(z))(V_\epsilon^{\text{rad}}(z)) \quad (46)$$

holds, see [40, Sec. 5.1]. Let $\tau_0 > 0$ be small enough such that $\omega_{\sqrt{\tau_0}}(z)$ does not intersect with other materials, i.e. $\partial\omega_{\sqrt{\tau_0}}(z) \cap (\partial\Omega_f \cup \partial\Omega_a) = \emptyset$. For $\tau \in (0, \tau_0]$, $\delta \in (-\tau, \tau_0 - \tau)$ we interpret $\Omega_{\sqrt{\tau+\delta}}(z) = (\text{id} + (\sqrt{\tau+\delta} - \sqrt{\tau})V_{\sqrt{\tau}}^{\text{rad}}(z))(\Omega_{\sqrt{\tau}}(z))$ as the deformation of $\Omega_{\sqrt{\tau}}(z)$ by $V_{\sqrt{\tau}}^{\text{rad}}$ as defined in (45). Using the shape differentiability of \mathcal{J} we conclude for the function $\hat{g}(\tau) = \frac{1}{|\omega|} \mathcal{J}(\Omega_{\sqrt{\tau}}(z))$

$$\begin{aligned} \hat{g}'(\tau) &= \lim_{\delta \rightarrow 0} \frac{\mathcal{J}(\Omega_{\sqrt{\tau+\delta}}(z)) - \mathcal{J}(\Omega_{\sqrt{\tau}}(z))}{|\omega|\delta} \\ &= \lim_{\delta \rightarrow 0} \frac{\mathcal{J}((\text{id} + (\sqrt{\tau+\delta} - \sqrt{\tau})V_{\sqrt{\tau}}^{\text{rad}}(z))(\Omega_{\sqrt{\tau}}(z))) - \mathcal{J}(\Omega_{\sqrt{\tau}}(z))}{\sqrt{\tau+\delta} - \sqrt{\tau}} \frac{\sqrt{\tau+\delta} - \sqrt{\tau}}{|\omega|\delta} \\ &= \lim_{t \rightarrow 0} \frac{\mathcal{J}((\text{id} + tV_{\sqrt{\tau}}^{\text{rad}}(z))(\Omega_{\sqrt{\tau}}(z))) - \mathcal{J}(\Omega_{\sqrt{\tau}}(z))}{t} \lim_{\delta \rightarrow 0} \frac{\sqrt{\tau+\delta} - \sqrt{\tau}}{|\omega|\delta} \\ &= d^S \mathcal{J}(\Omega_{\sqrt{\tau}}(z))(V_{\sqrt{\tau}}^{\text{rad}}(z)) \frac{1}{2|\omega|\sqrt{\tau}}, \end{aligned}$$

which exists since $\tau > 0$. Here we used the substitution $t = \sqrt{\tau+\delta} - \sqrt{\tau}$. For $\tau = 0$ we have similarly as in Lemma 2

$$\hat{g}'(0) = \lim_{\delta \searrow 0} \frac{\hat{g}(\delta) - \hat{g}(0)}{\delta} = \lim_{\epsilon \searrow 0} \frac{\mathcal{J}(\Omega_\epsilon(z)) - \mathcal{J}(\Omega)}{|\omega|\epsilon^2} = \frac{d}{d\Omega} \mathcal{J}(\Omega)(z).$$

Finally we show that the derivative is continuous in 0 by applying (46)

$$\begin{aligned} \lim_{\tau \searrow 0} \hat{g}'(\tau) &= \lim_{\tau \searrow 0} d^S \mathcal{J}(\Omega_{\sqrt{\tau}}(z))(V_{\sqrt{\tau}}^{\text{rad}}(z)) \frac{1}{2|\omega|\sqrt{\tau}} \\ &= \lim_{\epsilon \searrow 0} d^S \mathcal{J}(\Omega_\epsilon(z))(V_\epsilon^{\text{rad}}(z)) \frac{1}{2|\omega|\epsilon} = \frac{d}{d\Omega} \mathcal{J}(\Omega)(z) = \hat{g}'(0). \end{aligned}$$

□

Remark 22. The missing step to prove Corollary 1 for the general case of a quasilinear PDE constraint, which would cover our application, is the identity (46). It is, to our knowledge, still open and subject of ongoing research.

Funding

The work of the authors is partially supported by the joint DFG/FWF Collaborative Research Centre CREATOR (DFG: Project-ID 492661287/TRR 361; FWF:

10.55776/F90) at TU Darmstadt, TU Graz, JKU Linz and RICAM Linz. Further support is given by the Graduate School CE within the Centre for Computational Engineering at TU Darmstadt. P.G. is partially supported by the State of Upper Austria.

References

- [1] A. Alla, M. Hinze, P. Kolvenbach, O. Lass, and S. Ulbrich. A certified model reduction approach for robust optimal control with PDE constraints. *Advances in Computational Mathematics*, 45(3):1221–1250, June 2019.
- [2] G. Allaire, F. Jouve, and A.-M. Toader. Structural optimization using sensitivity analysis and a level-set method. *Journal of Computational Physics*, 194(1):363–393, 2004.
- [3] S. Amstutz and H. Andrä. A new algorithm for topology optimization using a level-set method. *Journal of Computational Physics*, 216(2):573–588, 2006.
- [4] S. Amstutz and P. Gangl. Topological derivative for the nonlinear magneto-static problem. *Electronic Transactions on Numerical Analysis*, 51:169–218, 2019.
- [5] A. Ben-Tal and A. Nemirovski. Robust optimization—methodology and applications. *Mathematical Programming*, 92(3):453–480, May 2002.
- [6] A. Ben-Tal and E. Roos. Beyond local optimality conditions: the case of maximizing a convex function. 2021.
- [7] M. P. Bendsøe. Optimal shape design as a material distribution problem. *Structural Optimization*, 1(4):193–202, 1989.
- [8] D. Bertsimas, O. Nohadani, and K. M. Teo. Nonconvex robust optimization for problems with constraints. *INFORMS Journal on Computing*, 22(1):44–58, 2010.
- [9] J. Birge and F. Louveaux. *Introduction to Stochastic Programming*. Springer Series in Operations Research and Financial Engineering. Springer New York, 2011.
- [10] G. Bramerdorfer, J. A. Tapia, J. J. Pyrhönen, and A. Cavagnino. Modern electrical machine design optimization: Techniques, trends, and best practices. *IEEE Transactions on Industrial Electronics*, 65(10):7672–7684, 2018.
- [11] F. Caubet, M. Dambrine, G. Gargantini, and J. Maynadier. Shape optimization under a constraint on the worst-case scenario. *SIAM Journal on Scientific Computing*, 46(6):A3703–A3726, 2024.

- [12] T. Cherrière, L. Laurent, S. Hlioui, F. Louf, P. Duysinx, C. Geuzaine, H. Ben Ahmed, M. Gabsi, and E. Fernandez. Multi-material topology optimization using wachspress interpolations for designing a 3-phase electrical machine stator. *Structural and Multidisciplinary Optimization*, 65, 11 2022.
- [13] F. H. Clarke. Generalized gradients and applications. *Transactions of the American Mathematical Society*, 205:247–262, 1975.
- [14] S. Conti, H. Held, M. Pach, M. Rumpf, and R. Schultz. Risk averse shape optimization. *SIAM Journal on Control and Optimization*, 49(3):927–947, 2011.
- [15] L. D’Angelo, Z. Bontinck, S. Schöps, and H. De Gersem. Robust optimization of a permanent magnet synchronous machine considering uncertain driving cycles. 07 2019.
- [16] J. M. Danskin. *The Theory of Max-Min and its Application to Weapons Allocation Problems*. Ökonometrie und Unternehmensforschung Econometrics and Operations Research. Springer Berlin, Heidelberg, 1967. Published: 01 March 2012 (Softcover), Published: 06 December 2012 (eBook).
- [17] M. Diehl, H. G. Bock, and E. Kostina. An approximation technique for robust nonlinear optimization. *Mathematical Programming*, 107(1-2, Ser. B):213–230, 2006.
- [18] D. Dyck and D. Lowther. Automated design of magnetic devices by optimizing material distribution. *IEEE Transactions on Magnetics*, 32(3):1188–1193, 1996.
- [19] H. Egger, M. Harutyunyan, R. Löscher, M. Merkel, and S. Schöps. On torque computation in electric machine simulation by harmonic mortar methods. *Journal of Mathematics in Industry*, 12(6), 2022.
- [20] A. El-Refaie and M. Osama. High specific power electrical machines: a system perspective. 2017.
- [21] P. Gangl. *Sensitivity-Based Topology and Shape Optimization with Application to Electrical Machines*. Dissertation, Johannes Kepler Universität, 2017.
- [22] P. Gangl, S. Amstutz, and U. Langer. Topology optimization of electric motor using topological derivative for nonlinear magnetostatics. *IEEE Transactions on Magnetics*, 52(3):1–4, 2016.
- [23] P. Gangl, U. Langer, A. Laurain, H. Meftahi, and K. Sturm. Shape optimization of an electric motor subject to nonlinear magnetostatics. *SIAM Journal on Scientific Computing*, 37(6):B1002–B1025, 2015.

- [24] P. Gangl and K. Sturm. Automated computation of topological derivatives with application to nonlinear elasticity and reaction–diffusion problems. *Computer Methods in Applied Mechanics and Engineering*, 398:115288, 2022.
- [25] C. Geiersbach, T. Suchan, and K. Welker. Stochastic augmented lagrangian method in riemannian shape manifolds. *Journal of Optimization Theory and Applications*, August 21 2024.
- [26] M. Goerigk, J. Kurtz, M. Schmidt, and J. Thürauf. Connections and reformulations between robust and bilevel optimization. 02 2024.
- [27] A. Henrot and M. Pierre. *Variation et optimisation de formes*, volume 48 of *Mathématiques & Applications (Berlin) [Mathematics & Applications]*. Springer, Berlin, 2005. Une analyse géométrique. [A geometric analysis].
- [28] Z. Houta, F. Messine, and T. Huguet. Topology optimization for magnetic circuits with continuous adjoint method in 3d. *COMPEL - The international journal for computation and mathematics in electrical and electronic engineering*, 43, 05 2024.
- [29] P. Kolvenbach, O. Lass, and S. Ulbrich. An approach for robust PDE-constrained optimization with application to shape optimization of electrical engines and of dynamic elastic structures under uncertainty. *Optimization and Engineering*, 19(3):697–731, 2018.
- [30] T. Komann, M. Wiesheu, S. Ulbrich, and S. Schöps. Robust design optimization of electric machines with isogeometric analysis. *Mathematics*, 12(9), 2024.
- [31] D. P. Kouri and T. M. Surowiec. Risk-averse pde-constrained optimization using the conditional value-at-risk. *SIAM Journal on Optimization*, 26(1):365–396, 2016.
- [32] N. Krenn and P. Gangl. Multi-material topology optimization of an electric machine considering demagnetization, 2024.
- [33] E. Kuci. *Shape and Topology Optimization for electro-mechanical energy converters*. Phd thesis, Université de Liège, 2018.
- [34] O. Lass and S. Ulbrich. Model order reduction techniques with a posteriori error control for nonlinear robust optimization governed by partial differential equations. *SIAM Journal on Scientific Computing*, 39(5):S112–S139, Oct. 2017.
- [35] B. S. Lazarov and O. Sigmund. Filters in topology optimization based on helmholtz-type differential equations. *International Journal for Numerical Methods in Engineering*, 86(6):765–781, 2011.

- [36] G. Lei, G. Bramerdorfer, C. Liu, Y. Guo, and J. Zhu. Robust design optimization of electrical machines: A comparative study and space reduction strategy. *IEEE Transactions on Energy Conversion*, 36(1):300–313, 2021.
- [37] S. Leyffer, M. Menickelly, T. Munson, C. Vanaret, and S. M. Wild. A survey of nonlinear robust optimization. *INFOR: Information Systems and Operational Research*, 58(2):342–373, 2020.
- [38] J. Martínez-Frutos, D. Herrero-Pérez, M. Kessler, and F. Periago. Robust shape optimization of continuous structures via the level set method. *Computer Methods in Applied Mechanics and Engineering*, 305:271–291, 2016.
- [39] F. Nishanth and B. Wang. Topology optimization of electric machines: A review. In *2022 IEEE Energy Conversion Congress and Exposition (ECCE)*, pages 1–8, 2022.
- [40] A. A. Novotny and J. Sokołowski. *Topological Derivatives in Shape Optimization*. Interaction of Mechanics and Mathematics. Springer Berlin, Heidelberg, 1 edition, 2013.
- [41] P. Putek, R. Pulch, A. Bartel, E. J. W. ter Maten, M. Günther, and K. M. Gawrylczyk. Shape and topology optimization of a permanent-magnet machine under uncertainties. *Journal of Mathematics in Industry*, 6(11), 2016.
- [42] N. Sadowski, Y. Lefevre, M. Lajoie-Mazenc, and J. Cros. Finite element torque calculation in electrical machines while considering the movement. *IEEE Transactions on Magnetics*, 28(2):1410–1413, 1992.
- [43] S. Sanogo and F. Messine. Topology optimization in electromagnetism using SIMP method. *COMPEL: The International Journal for Computation and Mathematics in Electrical and Electronic Engineering*, 37(6):2138–2157, Oct. 2018.
- [44] S. Sato, T. Sato, and H. Igarashi. Topology optimization of synchronous reluctance motor using normalized gaussian network. *IEEE Transactions on Magnetics*, 51(3):1–4, 2015.
- [45] J. Schöberl. C++ 11 implementation of finite elements in ngsolve. *Institute for analysis and scientific computing, Vienna University of Technology*, 30, 2014.
- [46] A. Shapiro, D. Dentcheva, and A. Ruszczyński. *Lectures on stochastic programming. Modeling and theory*. 01 2009.
- [47] G. Silva, N. Aage, A. Beck, and O. Sigmund. Three-dimensional manufacturing tolerant topology optimization with hundreds of millions of local stress

constraints. *International Journal for Numerical Methods in Engineering*, 122, 09 2020.

- [48] J. Sokolowski and J.-P. Zolésio. *Introduction to shape optimization*, volume 16 of *Springer Series in Computational Mathematics*. Springer-Verlag, 1992.
- [49] J. Wu, J. Gao, Z. Luo, and T. Brown. Robust topology optimization for structures under interval uncertainty. *Advances in Engineering Software*, 99:36–48, 2016.